Equatorial Atlantic variability and its relation to mean state biases in CMIP5

INGO RICHTER

Research Institute for Global Change and Application Laboratory, JAMSTEC, Yokohama, Japan, and Application Laboratory, JAMSTEC, Yokohama Japan

SHANG-PING XIE

International Pacific Research Center and Department of Meteorology, University of Hawaii at Manoa, Honolulu, Hawaii and Scripps Institution of Oceanography, University of California at San Diego, La Jolla, California

SWADHIN K. BEHERA AND TAKESHI DOI

Research Institute for Global Change, JAMSTEC, Yokohama, Japan, and Application Laboratory, JAMSTEC, Yokohama Japan

YUKIO MASUMOTO

Research Institute for Global Change, JAMSTEC, Yokohama, Japan

Climate Dynamics

submitted, 4 August 2012

revised, 21 November 2012

Corresponding author address:

Ingo Richter

Research Institute for Global Change, JAMSTEC, 3173-25 Showa-machi, Kanazawa-ku, Yokohama, Kanagawa 236-0001, Japan

E-mail: richter@jamstec.go.jp

ABSTRACT

Coupled general circulation model (GCM) simulations participating in the Coupled Model Intercomparison Project Phase 5 (CMIP5) are analyzed with respect to their performance in the equatorial Atlantic. In terms of the mean state, 29 out of 33 models examined continue to suffer from serious biases including an annual mean zonal equatorial SST gradient whose sign is opposite to observations. Westerly surface wind biases in boreal spring play an important role by deepening the thermocline in the eastern equatorial Atlantic and thus reducing upwelling efficiency and SST cooling in the following months. Both magnitude and seasonal evolution of the biases are very similar to what was found previously for CMIP3 models, indicating that improvements have only been modest. The weaker than observed equatorial easterlies are also simulated by atmospheric GCMs forced with observed SST. They are related to both continental convection and the latitudinal position of the Intertropical Convergence Zone (ITCZ). Particularly the latter has a strong influence on equatorial zonal winds in both the seasonal cycle and interannual variability. The dependence of equatorial easterlies on ITCZ latitude shows a marked asymmetry. From the equator to 15°N, the equatorial easterlies intensify approximately linearly with ITCZ latitude. This dependency vanishes when the ITCZ is located near to or south of the equator.

Despite serious mean state biases, several models are able to capture some aspects of the equatorial mode of interannual SST variability, including amplitude, pattern, phase locking to boreal summer, and duration of events. The latitudinal position of the boreal spring ITCZ, through its influence on equatorial surface winds, appears to play an important role in initiating warm events.

1. Introduction

The tropical Atlantic is characterized by significant interannual variability in sea-surface temperatures (SST) that exert an important influence on precipitation over the surrounding continents (Folland et al. 1986; Nobre and Shukla 1996). Two modes of SST variability are thought to exist (Xie and Carton 2004; Chang et al. 2006). One is the meridional mode (also inter-hemispheric gradient mode, meridional gradient mode, or dipole mode), with two centers of action in the subtropical north and south Atlantic (Hastenrath and Heller 1977). Studies have linked the meridional mode to a mechanism involving surface winds, evaporation, and SST (WES) feedback (Xie and Philander 1994; Chang et al. 1997).

The second mode of tropical Atlantic variability involves the equatorial cold tongue region, which is centered just south of the equator in the eastern part of the basin. This mode, usually referred to as the zonal mode (also equatorial mode), is thought to be governed by dynamics similar to those responsible for El Nino/Southern Oscillation (ENSO) in the equatorial Pacific (e.g. Servain et al. 1982; Zebiak 1993; Keenlyside and Latif 2007).

In terms of the mean state, the equatorial Atlantic resembles the equatorial Pacific in many aspects. Both basins feature a warm pool in the west, a cold tongue in the east, and mean surface easterlies that drive an eastward equatorial current year round. Consistent with the surface winds, water piles up at the western boundary. This is associated with a deep mixed layer that insulates the surface from cold sub-thermocline waters and thus helps to maintain warm SST. Conversely, the eastern basin is characterized by a shallow thermocline that makes the SST very sensitive to variations in equatorial upwelling.

The eastern equatorial Atlantic features a pronounced seasonal cycle. According to OISST climatology, SST averaged in the eastern basin (20°W-0 and 3°S-3°N) drops from approximately 29°C in April to 24.5°C in August as the cold tongue develops. Studies have linked the seasonal cold tongue development to the onset of the African monsoon and associated cross-equatorial surface winds over the eastern basin (Mitchell and Wallace 1992; Okumura and Xie 2004; Caniaux et al. 2011), which produce upwelling just south of the equator (Philander and Pacanowski 1981).

The strong seasonality of the Atlantic cold tongue influences interannual variability. Thus warm events (Atlantic Niños) preferentially occur during boreal summer and are associated with reduced cold tongue development (Carton and Huang 1994). The SST amplitude of these events is about 1K (roughly one third of their Pacific counterparts), which is much smaller than the ~5K amplitude of the seasonal cycle. Therefore Atlantic Niños can be described as a modulation of the seasonal cycle (Philander 1986), which may help to explain their phase locking to boreal summer.

While monsoon-related cross-equatorial winds may govern cold tongue development in the climatological sense, interannual variability is significantly influenced by remote forcing from western equatorial surface winds (Keenlyside and Latif 2007). Weakening of the equatorial easterlies has been shown to excite Kelvin waves that propagate eastward and reduce the slope of the equatorial thermocline (Servain et al. 1982; Hormann and Brandt 2009) though not all events may be dominated by this mechanism (Carton and Huang 1994). The relatively small size of the Atlantic basin implies that the major wind stress forcing region (~40°W) and the cold tongue region (10°W) are only separated by about 30° of longitude or roughly 3300 km. In the equatorial Atlantic, the second baroclinic Kelvin wave mode is considered to be dominant (e.g. Doi et al. 2007; Polo et al. 2008) and its phase speed has been estimated to be

1.2-1.5 m/s (Du Penhoat and Treguier 1985; Philander 1990; Katz 1997; Franca et al. 2003; Illig et al. 2004; Guivarc'h et al. 2008). Thus Kelvin waves excited by western equatorial wind stress anomalies reach the cold tongue region in about one month. Observational studies, however, indicate a wide range of delay times from 1-2 months (Servain et al. 1982; Keenlyside and Latif 2007) to 4-6 months (Hisard et al. 1986; Vauclair and du Penhoat 2001; Chang et al. 2006). Thus the lag implied by Kelvin wave propagation is at the lower end of observational estimates. This suggests that rather than influencing SST directly, the remotely forced Kelvin waves might precondition the eastern equatorial thermocline in boreal spring (Hormann and Brandt 2009). When the seasonal cold tongue development starts in boreal summer these subsurface anomalies are upwelled to the surface and influence SST.

The above description indicates the possibility of a positive feedback involving western equatorial Atlantic surface winds, cold tongue SST, and thermocline depth, similar to the Bjerknes feedback in the equatorial Pacific (Zebiak 1993). Indeed, several studies have indicated that the Bjerknes feedback plays an important role in the Atlantic as well (Keenlyside and Latif 2007; Ding et al. 2010). The study by Ding et al. also shows evidence for a 90-degree-out-of-phase relationship between equatorial upper ocean heat content and cold tongue SST, which is a central component of the so-called discharge-recharge oscillator paradigm (Jin 1997). This lead-lag relation between heat content and SST is fundamental to the successful prediction of ENSO and has allowed skillful predictions at 12 months lead-time and beyond (Luo et al. 2008). Ding et al. (2010) suggest that knowledge of equatorial Atlantic heat content should enable skillful prediction up to 3 months ahead.

Actual seasonal prediction in the equatorial Atlantic, however, does currently not live up to this expectation. In most cases dynamic models are matched or even outperformed by persistence and statistical models (Stockdale 2006). Reasons for this poor performance are manifold but mean state biases are certainly a factor. While general circulation models (GCMs) give a relatively reasonable representation of the tropical Pacific climate (de Szoeke and Xie 2008), they suffer from severe biases in the tropical Atlantic (Davey et al. 2002; Richter and Xie 2008 (hereafter RX08); Richter et al. 2012). One of the most obvious shortcomings is the GCMs' inability to adequately capture the boreal summer cold tongue development. This warm bias in the eastern basin is accompanied by colder than observed SSTs in the west and manifests as a reversal of the annual mean SST gradient along the equator (Davey et al. 2002; RX08). Several studies suggest that the lack of cold tongue development in boreal summer is at least partly due to westerly wind stress biases in boreal spring (Chang et al. 2007, 2008; RX08; Wahl et al. 2009; Tozuka et al. 2010; Richter et al. 2012). Such wind biases deepen the eastern equatorial thermocline and thus reduce the impact of eastern equatorial upwelling in JJA.

The MAM westerly biases are common in GCMs and occur even when the models are forced with observed SSTs (RX08). This suggests that the atmospheric GCM (AGCM) components play a large role in the persistent tropical Atlantic SST biases. Richter et al. (2012) show that continental precipitation biases are one of the factors controlling the simulated equatorial easterlies. In particular, they find that deficient and excessive precipitation over the Amazon and Congo basins, respectively, are accompanied by a weakened Atlantic Walker circulation and westerly surface wind biases.

While continental precipitation plays some role in the strength of the equatorial easterlies, the latitudinal position of the Atlantic Intertropical Convergence Zone (ITCZ) appears to be another factor. Several studies have shown that even AGCMs with specified observed SSTs tend to place the ITCZ south of the equator in MAM, whereas in observations it is mostly on or north of the equator (Biasutti et al. 2006; RX08; Tozuka et al. 2011). In the present study we will show that there is a very high correspondence between the latitudinal ITCZ position and the strength of the equatorial easterlies on the equator.

The present study has two main goals. The first is to re-examine the performance of GCMs using output from the Coupled Model Intercomparison Project Phase 5 (CMIP5) and observations. In particular we investigate whether the MAM surface wind mechanism found to be crucial in CMIP3 by RX08 still plays a dominant role in developing boreal summer cold tongue biases in CMIP5 models.

The second goal is to analyze the zonal mode of variability in both observations and CMIP5 simulations. First we examine observations and reanalyses to characterize the evolution of Atlantic Niños in terms of surface winds, thermocline depth, and SST. We are particularly interested in reexamining the lag between western equatorial surface wind forcing and cold tongue SST response. We then assess to what extent CMIP5 models are able to simulate the zonal mode and how this is related to their mean state biases. To our surprise, some models are able to reproduce at least some aspects of observed variability despite their substantial mean state biases.

The observational data and model output used in this study are described in section 2. Mean state biases are the focus of section 3, while interannual variability is examined in section 4. Section 5 discusses our results regarding mean state and interannual variability of the equatorial Atlantic. Section 6 presents our conclusions.

2. CMIP5 and observational data sets

We use model output from the CMIP5 integrations. Since we are investigating natural variability our emphasis will be on the pre-industrial control simulations (experiment piControl) with climatological greenhouse gas forcing corresponding to pre-industrial values. Comparing these to present day observations introduces a small error due to the different greenhouse gas concentrations. Due to the severity of the biases, this error is negligible in most models. Where the error is not negligible it tends to make the model biases appear slightly less severe than they actually are (see also Richter et al. 2012). At the time of analysis 33 models were available for downloading. Four of these use flux corrections and have been eliminated from some of the analysis, including the calculation of ensemble means and inter-model correlations. We also neglect models with carbon cycle and chemistry if a more basic version exists in the database and is sufficiently similar in terms of its tropical Atlantic simulation. Thus we include, e.g., the Japanese model MIROC-ESM but exclude the version with added chemistry calculations, MIROC-ESM-CHEM. The remaining models are used to calculate two ensemble means. Ensemble MOST includes all the remaining models, while ensemble AN includes only those that achieve a somewhat realistic representation of Atlantic Niños. Table 1 lists the 33 models used in this study and the members of the two ensembles. In some cases, to highlight the differences between AN and other models, we use an ensemble made up of all MOST models except those that are part of AN (MOST-AN).

While our focus is on the pre-industrial control simulations we also consider the atmospheric simulations forced with observed SST (experiment AMIP) in order to analyze the AGCM contribution to coupled model errors.

Model output is compared with several observational datasets. For SST we use the Reynolds optimally interpolated dataset (OISST; Reynolds et al. 2002) for the period 1982-2010. Precipitation for the period 1979-2010 is from the Global Precipitation Climatology Project (GPCP) version 2.2, which is a blend of station and satellite data (Adler et al. 2003). Surface winds are from the international comprehensive ocean-atmosphere dataset (ICOADS; Woodruff et al. 2010; period 1960-2010), which relies on ship observations. Recently Tokinaga and Xie (2011) have devised a scheme to correct the ICOADS near-surface wind observations for spurious trends due to changes in anemometer height. We use this Wave and Anemometer-Based Sea Surface Wind (WASWind) dataset for both climatology and interannual variability. Thermocline depth is calculated using the World Ocean Atlas (WOA) 2005 climatological ocean temperature (Locarnini et al. 2006).

We also make use of atmospheric and oceanic reanalysis datasets, which have the advantage of providing a gap-free and physically consistent set of variables. On the atmospheric side we use National Center for Environmental Prediction/National Center for Atmospheric Research (NCEP/NCAR) reanalysis (Kalnay et al. 1996; period 1948-2010), European Centre for Medium-Range Weather Forecasts (ECMWF) 40-year Reanalysis (ERA40; Uppala et al. 2005; period 1958-2001), and the ECMWF Interim Reanalysis (ERA Interim; Dee et al. 2011; period 1989-2010). For oceanic fields we rely on the Simple Ocean Data Assimilation (SODA) reanalysis (Carton et al. 2000; period 1958-2006).

All datasets were subjected to linear detrending before anomalies were calculated. This is important for the observational datasets, which contain significant trends over the observation period, but also for some of the piControl datasets, which feature spurious trends due to top-of-atmosphere radiative imbalance. Detrending is also necessary for the AMIP simulations since these are forced with observed SST from 1978-2008.

3. Mean state model biases

The starting point of our analysis is the annual mean SST along the equator, averaged between 2°S-2°N (Fig. 1a). For comparison we also show the same field for the CMIP3 models in Fig. 1b (this Figure is identical to the one in RX08, except that the observations are OISST instead of ICOADS). The general impression is that the models continue to suffer from severe equatorial SST biases although the spread seems to have reduced to some extent. Most models feature a zonal SST gradient that is of opposite sign relative to observations. Nevertheless, a few models are able to reproduce the observed SST minimum in the eastern basin around 10°W. These are the BNU-ESM, HadGEM2-CC, HadGEM2-ES, and the MRI-CGCM3. Even those, however, continue to suffer from colder than observed SST in the warm pool region. All models examined are too cold in the west, and most too warm in the east. We note that in addition to the gradient bias, there is also an offset error in the tropical mean SST of a given GCM (Li and Xie 2012), which we do not discuss here.

In terms of seasonal evolution, biases first appear in the equatorial trades in MAM (Fig. 2). The weaker than observed surface wind stress is followed by an erroneous deepening of the thermocline with maximum errors in June. This subsurface temperature anomaly becomes apparent at the surface when upwelling strengthens in boreal summer. The maximum SST error occurs in July, one month after the peak in thermocline depth error. This evolution is consistent with the results of RX08 and underscores the robustness of this mechanism.

As in RX08, the MAM westerly wind bias already exists in the AMIP simulations (Fig. 3) with SSTs prescribed from observations, indicating that one of the root causes for the biases lies in the atmospheric components of the models. Figure 3 suggests that the westerly surface wind bias is related to both deficient precipitation over the Amazon region and excessive marine precipitation south of the equator. The dry bias over South America has already been examined in several studies, including RX08, Tozuka et al. (2011), and Richter et al. (2012). Figure 4a gives a quantitative summary of this relation by plotting the climatological MAM precipitation averaged over (70-40°W, 0-5°N, ocean points excluded) versus the MAM equatorial wind stress over the ocean (40-10°W, 2°S-2°N), with each letter representing one model. This reveals an approximately linear relation between a model's north equatorial Amazon precipitation and its equatorial wind stress. A few models, however do not seem to follow this relation resulting in a relatively low inter-model correlation of -0.39. For the coupled piControl runs this correlation is higher (-0.53, not shown), which is likely due to the error intensification in the coupled GCMs.

The southward shift of the marine ITCZ (Fig. 3) is a well-documented feature that is common to most GCMs (Mechoso et al. 1995) and occurs in both the Atlantic and Pacific basins. It is sometimes referred to as the double-ITCZ problem. While the majority of studies have examined this problem in the Pacific basin (e.g. Lin 2007; deSzoeke and Xie 2008; Belluci et al. 2010), a few have also examined its Atlantic counterpart, e.g. Biasutti et al. (2006). To our knowledge, the impact of the southward ITCZ shift on the equatorial easterlies has not been discussed in detail. An AMIP inter-model scatter plot of climatological south-of-the-equator precipitation (averaged from 40°W-10°E, 10-4°S) versus climatological equatorial zonal wind stress (Fig. 5a) suggests some correspondence between the two fields. Two obvious outliers are the atmospheric components of MRI-CGCM3 and GISS-E2-R. With these removed the correlation increases to 0.57 (vs. 0.36 when all models are included). For the coupled piControl runs the inter-model correlation is 0.60 with all models included (Fig. 5b), and 0.86 after excluding three outliers (GISS-E2-H, GISS-E2-R, and EC-EARTH).

We further investigate the relation between wind and precipitation by plotting the zonal equatorial wind stress as a function of ITCZ latitude (Fig. 6). piControl simulations are used since they exhibit a wider range of ITCZ variability, due to the freely evolving SST and the longer integration time. Here, ITCZ latitude is calculated for each month of the respective dataset by zonally averaging precipitation from 40°W to 10°E and determining the latitude of the precipitation maximum. The relation is fairly similar in models and the ERA Interim, with the least negative wind stress (i.e. the weakest easterlies) occurring when the ITCZ is located at around 3°S. For some models this wind stress maximum lies closer to or on the equator, e.g. the MRI-CGCM3 (not shown). Note that the zonal wind response is not symmetric with respect to the ITCZ latitude. The equatorial easterlies rapidly intensify as the ITCZ moves north of the equator but remain weak as it moves south of the equator.

The equatorial wind response to ITCZ positions on and north of the equator can be understood in terms of the surface momentum balance (Okumura and Xie 2004; Ogata and Xie 2011). As the ITCZ shifts further north so do the southeasterly trades. Thus meridional winds advect easterly momentum toward the equator and strengthen the equatorial easterlies. This mechanism, however, cannot account for the latitudinal asymmetry of the response. More detailed analysis will be needed to understand this behavior, including consideration of meridional asymmetries of the ITCZ.

The sensitivity of the equatorial winds to the ITCZ latitude suggests that the erroneous southward ITCZ shift in most GCM simulations is intricately linked to the westerly surface wind biases. The erroneous southward shift, in turn, is at least partly independent of the SST biases since AGCMs forced with prescribed SSTs also exhibit this problem to some extent (Fig. 4; see also Biasutti et al. 2006; RX08; Tozuka et al. 2011). In the coupled context the meridional asymmetry of the surface wind response to the ITCZ location (Fig. 6) may provide a positive feedback that helps to lock the ITCZ into a south-equatorial position: as the ITCZ approaches the equator from the northern hemisphere (typically in boreal spring) the equatorial easterlies weaken, thereby reducing upwelling and warming SST where the thermocline is shallow. Warmer SST on the equator, however, facilitates deep convection there, further pulling the ITCZ equatorward. Once the ITCZ is centered on the equator cross-equatorial surface winds will be close to zero, thereby shutting off the associated upwelling and cooling just south of the equator (Philander and Pacanowski 1981). This is somewhat analogous to the WES feedback but relies on equatorial upwelling rather than evaporation as the feedback link.

4. Observed and simulated interannual variability

4.1. Evaluation of CMIP5 performance

We assess interannual SST variability by performing an EOF analysis. Since the zonal mode is most active during boreal summer we compute EOFs based on JJA seasonal means. All datasets were detrended prior to analysis. We focus on the models in ensemble AN and only show the ensemble mean for the remaining models. The first EOF mode in the HadISST dataset shows positive loadings along the eastern equator (approximately 20°W-0) and extending southeastward toward the southwest African coast (Fig. 7). The southeastward branch shows the signature of Benguela Niños, which are interannual warm anomalies in the Benguela upwelling region (Shannon et al. 1986; Florenchie et al. 2003). Benguela Niños tend to peak in boreal spring and commonly precede Atlantic Niños (Florenchie et al. 2003; Luebbecke et al. 2010; Richter et al. 2010). This tendency is documented by the EOF analysis, which captures the decaying phase of the Benguela Niño. The first EOF mode explains 29% of the JJA SST variance in the HadISST (Rayner et al. 2003; analysis period 1950-2010).

In the CMIP5 piControl runs some models seem to be able to capture the zonal mode structure in their first EOF (Fig. 7). The Beijing Climate Center and Bergen Climate Center models compare favorably with the observations in terms of both amplitude and pattern. The GFDL and Hadley Centre models capture the pattern fairly well but overestimate amplitude. The MRI model has fairly realistic amplitude but shifts the center too far west and underestimates the Benguela Nino signature. Finally, the Australian ACCESS1-3 model produces too elongated a pattern along the equator. The remaining models (grouped into ensemble MOST-AN) produce an SST pattern that lacks a pronounced equatorial signature and is indicative of basin wide warming. We note that some of the MOST-AN models feature an Atlantic Niño pattern in their second EOF (e.g. CCSM4; not shown), indicating that the zonal mode does exist in those GCMs but is not dominant. Almost all the GCMs examined do not feature a pronounced peak in cold tongue variability outside boreal summer (not shown), though some feature a secondary maximum in November, which is consistent with observations (Okumura and Xie 2006).

For the observations, reanalysis, and ensemble means, we show surface wind and precipitation regressed on the first principal component of SST. Except for ensemble MOST-AN, the patterns show positive precipitation anomalies over the Gulf of Guinea and extending into the coastal regions of Northwest Africa. Both ensemble AN and ERA40 indicate intense surface wind convergence that this is collocated with the center of the precipitation anomalies in the Gulf of Guinea. In the observations, on the other hand, surface wind convergence and precipitation are weaker and shifted further west. All three datasets show westerly wind anomalies on the equator that are indicative of the Bjerknes feedback. The SST, surface wind and precipitation patterns compare relatively well with previous observational studies (e.g. Ruiz-Barradas et al. 2000; Okumura and Xie 2006).

4.2. Preconditioning of the eastern equatorial Atlantic by MAM easterlies

As discussed in the introduction section, the weakening of the equatorial easterlies during boreal spring is an important factor in the development of Atlantic Niños. Richter et al. (2012) have shown that many CMIP3 models feature a strong correlation between MAM zonal surface wind and JJA cold tongue SST anomalies. In the following we examine the preconditioning role of the surface winds in more detail.

Longitude-time sections of seasonally stratified standard deviation along the equator (Fig. 8) indicate a peak of SST variability in June and June/July for ERA Interim and ERA 40, respectively. The equatorial easterlies, on the other hand, are most variable in May. Thus maximum wind variability precedes maximum SST variability, which cannot be explained by the SST-wind component of Bjerknes feedback (i.e. the influence of eastern equatorial Atlantic SST on western equatorial Atlantic winds). The models show similar patterns of variability (Fig. 8c) but the peak of SST variability occurs in July and extends further westward than observed. The simulated wind stress variability is most pronounced in May, as in the reanalyses, but its maximum is located eastward toward the center of the basin, while the reanalyses produce maximum variability close to the South American coast. Ensemble AN (Fig. 8d) differs from ensemble MOST mostly in amplitude, not in pattern. Thus the models with relatively realistic Atlantic Niños feature stronger variability in both surface winds and SST. The temporal separation between surface winds and SST is more obvious in the models, as the May maximum of wind variability occurs when SST variability is still low.

Motivated by the lag between surface wind and SST variability, we calculate the correlation between MAM zonal surface wind stress in the equatorial Atlantic (40-10°W, 2°S-2°N) and JJA SST in the Atlantic cold tongue region (ACT1; 15-5°, 3°S-3°N) for ICOADS observations, reanalyses, and CMIP5 piControl simulations (Fig. 9a). The reanalysis datasets feature correlations ranging from approximately 0.42 (NCEP reanalysis) to 0.68 (ERA Interim), with the ICOADS observations somewhere in between at 0.53. The high correlation in ERA Interim might be partly due to the particular period (1989-2010). ERA40 and NCEP feature higher correlations when restricted to this period (0.79 and 0.58, respectively), but ICOADS remains low (0.45).

For models, the correlation typically ranges from 0.5 to 0.8, though in some cases it is much lower. The two GISS models, e.g., have a correlation close to 0. This is probably at least partly related to their excessively deep thermocline, which is located at about 80m in the cold tongue region during boreal spring, 20m deeper than the observations suggest (not shown). Another model, EC-EARTH, features a negative correlation (-0.24) though we will not analyze the reasons for this behavior here.

We analyze the evolution of Atlantic Niños through a composite analysis keyed on ACT1 SST. Years for which the JJA SST anomaly exceeds 1.5 standard deviations are chosen for the composites. The ICOADS observations suggest that the weakening of the equatorial westerlies and the warming of the cold tongue SSTs occur almost simultaneously (Fig. 10a), though the wind anomalies drop off before SST peaks. The ERA40 and SODA reanalyses agree with this simultaneous evolution while the ERA Interim reanalysis suggests that surface winds lead by one month.

We categorize Atlantic Niños into two types based on the evolution of surface wind and SST anomalies. The one-stage type features simultaneous evolution of equatorial zonal surface winds, and cold tongue thermocline depth and SST (see Table 3 for a list of models). In the two-stage type, on the other hand, wind and thermocline depth anomalies lead SST anomalies by one to three months. These results from the composites are confirmed by a lagged correlation analysis (not shown).

The ERA Interim composite suggests a two-stage Atlantic Niño with a 1-month lag between wind and SST, and is therefore at odds with the other observational and reanalysis datasets. Limiting the other reanalysis datasets to the ERA Interim period (1989-2010) does not reconcile the differences. This could suggest a problem either with data quality or the reanalysis model. Studies of individual warm events (see introduction) suggest that both types do occur (e.g. 1984 vs. 1988 as discussed by Carton et al. 1994). Thus compositing might conflate the two types of events. A detailed analysis of individual events should be performed to resolve this but is beyond the scope of the present study.

Most models feature two-stage Atlantic Niños. This includes all the models that are able to capture the structure of equatorial Atlantic variability (see section 4.1) except ACCESS1-3. Other models with a one-stage evolution have a very deep thermocline in the eastern equatorial Atlantic (most notably GISS-E2-R and INMCM4), which might explain their apparent insensitivity to surface wind forcing.

One-stage Atlantic Niños, as seen in the ICOADS, ERA40, NCEP, and SODA datasets, are consistent with the SST-wind component of the Bjerknes feedback since the atmospheric winds can quickly adjust to SST anomalies. Oceanic adjustment to SST induced winds (the oceanic component of the Bjerknes feedback) should take at least one month as discussed in the introduction. This suggests that one-stage Atlantic Niños are triggered by local processes (e.g. oceanic Ekman divergence as suggested by Zebiak 1993), with remotely forced Kelvin waves amplifying the anomalies.

In two-stage Atlantic Niños, on the other hand, wind forcing in the west precedes the SST response. This indicates that these events are triggered by wind anomalies and subsequently amplified by the atmospheric component of the Bjerknes feedback. Some models feature a lag between wind and SST that is longer than one month. This cannot be explained by Kelvin wave propagation alone. Rather it suggests that the Kelvin wave signal acts to precondition the cold tongue region by deepening the thermocline (as suggested, e.g., by Hormann and Brandt 2009). The long delay time can be explained by the climatological cycle of upwelling cold tongue region, which rapidly intensifies in May and June. A westerly wind burst in April, e.g., will deepen the cold tongue thermocline in May, but its SST expression might not appear until June when upwelling intensifies. This is analogous to the bias evolution discussed by RX08. The mechanism implies that the delay between wind stress forcing and SST response is closely tied to the timing of the wind burst in relation to the seasonal cycle.

4.3. Variability of the ITCZ latitude and its role in Atlantic Niños

In section 3 we have shown that equatorial westerly wind biases are closely related with a southward shifted ITCZ in the climatological sense. Thus models with strong precipitation south of the equator also feature serious westerly biases on the equator in boreal spring. Here we would like to examine whether this relation also plays a role in interannual variability in either observations or GCMs. The Atlantic Niño composites (Fig. 10) indicate a close correspondence of south-equatorial precipitation anomalies and westerly wind anomalies on the equator in the ERA Interim reanalysis. The piControl simulations show a similar relation between the two fields (Figs. 10ef).

To obtain a more comprehensive view of the dynamics associated with south-equatorial precipitation anomalies, we composite anomalies of precipitation, surface wind vectors, and SST on equatorial westerly wind anomalies exceeding 2.5 standard deviations during boreal spring (MAM). The AN ensemble mean over composites (Fig. 11b) shows a precipitation dipole with positive values south of the equator between 30°W and the African coast, and negative values to the west and north. The precipitation anomalies are accompanied by a weakening of the South Atlantic subtropical high, as evidenced by the cyclonic surface wind anomalies (Fig. 11b). Close to the equator, northwesterly surface wind anomalies are prominent. Overall, the structure is quite similar to the mean state biases in the AMIP runs (Fig. 3) except that continental signals are weak and that the south-equatorial lobe is shifted to the east. In the ERA40 reanalysis there is some indication that southward shifts of the Atlantic ITCZ are linked to dry anomalies over northern South America and the eastern tropical Pacific between 0-10ºN (Fig. 11a). Such a link is not evident in the GCM ensemble mean (Fig. 11b) though it does feature to some extent in individual models (not shown). Thus the GCM analysis does not indicate that continental precipitation has a dominant influence on interannual south-equatorial ITCZ excursions and concomitant westerly wind anomalies.

The ensemble mean SST anomaly pattern in Fig. 11a indicates cooling (warming) north (south) of the equator, consistent with the precipitation anomalies and indicative of the meridional gradient mode. The ERA40 reanalysis (Fig. 11a) presents a qualitatively similar picture. Thus both reanalysis and GCMs suggests a link between the meridional and zonal mode, in which a pre-existing meridional SST gradient in boreal spring shifts the ITCZ and trade wind system southward, thus inducing westerly wind anomalies on the equator. This, in turn, deepens the eastern equatorial thermocline and sets the stage for an Atlantic Niño in boreal summer. Such a mechanism has been discussed by Servain et al. (1999, 2000). A simple correlation of MAM meridional mode and JJA zonal mode indicates relatively weak values for observations and reanalyses that range from 0.3 to 0.4 (Fig. 9b). In the piControl runs this correlation tends to be higher, particularly for the AN models.

Note that there is no clear correspondence between the spatial patterns of precipitation and SST anomalies. While the precipitation anomalies are most pronounced in the center of the basin, the SST anomalies tend to be closer toward the African coast both north and south of the equator. Certainly, the mean state SST plays an important role in shaping the pattern of precipitation anomalies; sensitivity of precipitation will be weak where SST is below the threshold for deep convection.

5. Discussion

5.1. Mean state biases

Our analysis of CMIP5 model performance in the tropical Atlantic indicates that, over all, improvement since CMIP3 (RX08) has only been modest. In fact, the ensemble mean biases (Figs. 2 and 3) appear almost identical to those discussed by RX08 in terms of both pattern and magnitude. One should keep in mind that the model sets in RX08 and the present study are different so that comparing the two ensembles can give only a rough impression of the improvement (or lack thereof) since CMIP3. In fact, the Hadley Centre and MRI models have achieved substantial improvement over respective earlier versions and eliminated a significant portion of their equatorial Atlantic biases. Apart from these two CMIP5 models, there have recently been two other coupled GCMs with a rather realistic representation of the tropical Atlantic mean state (see Richter et al. 2010 and Tozuka et al. 2011 for results from these models). This suggests that tropical Atlantic biases can be overcome even in the absence of fundamental changes in terms of parameterization approach or resolution (see also Wahl et al. 2011). Despite these few positive developments the overall lack of progress is somewhat disappointing. The reason might be related to the fact that many modeling centers have focused their CMIP5 efforts on adding new components, such as dynamic vegetation, chemistry, and carbon cycle, in order to perform the required experiments. It remains an open question if mean state biases have a substantial impact on climate projections but if so it might be crucial to intensify efforts on improving basic model performance before adding complexity. Another obstacle to progress in the tropical Atlantic might be that its problems are, in some sense, opposite to those in the tropical Pacific. Most models underestimate cold tongue SSTs in the Pacific while severely overestimating them in the Atlantic. Likewise, the equatorial easterlies are overestimated over the Pacific but underestimated over the Atlantic. Thus attempting to remedy problems in one basin can easily exacerbate them in the other. Modifications designed to reduce the Pacific equatorial easterlies, e.g., are likely to also reduce them over the Atlantic and thus further worsen SST biases there.

The seasonal evolution of surface wind, thermocline depth, and SST biases in the equatorial Atlantic (Fig. 2) is similar to that found by RX08 and thus suggests that a similar mechanism is responsible for the biases: surface winds in boreal spring deepen the eastern equatorial thermocline and thus increase subsurface temperatures. This reduces SST cooling during the main upwelling season in boreal summer. RX08 found that the surface wind biases already exist in uncoupled AGCMs forced with observed SST, and that they were related to both continental and oceanic precipitation biases. While RX08 and Richter et al. (2012) examined the role of continental precipitation biases, here we propose an additional mechanism that emphasizes the role of the erroneous southward shift of the marine ITCZ. Both problems appear to originate in the atmospheric model components but the surface wind biases appear to be more directly linked to ITCZ latitude than to continental precipitation. Doi et al. (2012) report similar results for two versions of the GFDL coupled GCM.

While we have emphasized here the role of the atmospheric model components in generating coupled model biases, this does not mean we discount other error sources. Rather we have followed one promising lead but other model shortcomings, such as e.g. diffuse thermoclines in the oceanic components, are likely to contribute and should be studied carefully.

5.2. Interannual variability

Despite substantial mean state biases several models are able to reproduce observed equatorial variability to some extent, including pattern, magnitude, preferred occurrence in boreal summer, and duration of the event (see Fig. 10). This represents a substantial improvement over CMIP3 models, most of which failed to represent the zonal mode adequately (Breugem et al. 2006). Of course, room for improvement remains even for the more successful models. A common difference between observations and models is that the latter produce maximum zonal mode variability in July or August, which is 1-2 months later than observed. This delayed onset is paralleled by the cold tongue thermocline depth, which reaches its annual minimum 1-2 months later than observed (August/September vs. July; not shown). As RX08 and the present study show, the thermocline depth evolution is very sensitive to western equatorial wind stress forcing, which in turn relates to the latitude of the ITCZ (see section 3). Latitude-time sections of precipitation and wind stress (Fig. 12) indicate that the latitudinal migration of the western Atlantic ITCZ is much more pronounced in the models than in observations. In observations the range is 0-8°N (April vs. August), while in the coupled model ensemble average it is 6°S-8°N (March vs. September). From May to June the simulated ITCZ jumps from a south-equatorial to a north-equatorial position, which is accompanied by a strong increase in equatorial easterlies. Thus the exaggeration of the ITCZ latitude range might contribute to the delayed onset of simulated cold tongue season and interannual variability.

While the simulated interannual SST variability in some models compares fairly well with observations, its relation to equatorial surface wind forcing appears to be different from that observed. In the models the evolution of Atlantic Niños occurs in two distinct phases. In the first phase westerly wind anomalies deepen the thermocline in the eastern equatorial Atlantic. In the second phase the subsurface temperature anomalies are brought to the surface by seasonal upwelling. This two-phase evolution typically involves a 1-3 month delay between surface wind anomalies and maximum SST response. Observations and reanalyses, on the other hand, suggest a one-phase evolution of Atlantic Niños, in which westerly wind, thermocline depth, and SST anomalies increase more or less simultaneously (in a monthly average sense). This might imply a deficiency in the simulated mechanism for interannual variability, likely related to the delayed cold tongue onset. On the other hand, it is possible that surface wind observations do not provide enough spatio-temporal coverage and accuracy to depict the evolution of Atlantic Niños. In addition, a recent study by Richter et al. (2012) suggests that there are large differences among observed events in terms of the evolution of wind and SST anomalies, with some events featuring a well-defined two-phase evolution. Such differences cannot be captured by compositing and will require a more detailed analysis.

6. Conclusions

We have investigated the mean state and interannual variability of the equatorial Atlantic simulated by GCM simulations participating in the CMIP5 intercomparison. Mean state biases continue to pose a serious problem for most (though not all) of the coupled GCMs analyzed here. The seasonal evolution of model biases follows the same pattern as discussed for CMIP3 (RX08), which involves weakening of the equatorial easterlies in boreal spring, subsequent deepening of the eastern equatorial thermocline, and maximum cold tongue SST bias during the boreal summer upwelling season. MAM surface wind biases are incipient in the atmospheric model components forced with observed SST. They are associated with precipitation biases over the adjacent landmasses and a southward shift of the marine ITCZ. Particularly the ITCZ bias is closely linked to equatorial winds both in terms of inter-model spread and interannual variability.

Regarding interannual variability, we find that despite their mean state biases several GCMs show reasonable performance in reproducing observed patterns, amplitude, and phase locking of SST anomalies. Thus mean state biases do not necessarily preclude interannual equatorial Atlantic variability with realistic features. The simulated phase relation between surface wind and SST anomalies features a 1-3 month lag between the two fields when warm events are composited. This does not show in the composites of observations and reanalyses where these fields vary more or less simultaneously.

In both models and observations, Atlantic Niños are associated with south-equatorial excursions of the marine ITCZ, which are accompanied by northwesterly surface wind anomalies on the equator. The wind anomalies, in turn, can induce warm SST anomalies on and just south of the equator through their influence on oceanic upwelling. This suggests a positive feedback for the development of interannual SST anomalies. Since the ITCZ position is also dependent on the more remote subtropical Atlantic SST north and south of the equator, there is an obvious pathway for the meridional mode to influence the zonal mode.

Acknowledgments

We thank the anonymous reviewers for their helpful comments. We acknowledge the World Climate Research Programme's Working Group on Coupled Modelling, which is responsible for CMIP, the U.S. Department of Energy's Program for Climate Model Diagnosis and Intercomparison which provides coordinating support and led development of software infrastructure for CMIP, and the climate modeling groups for making available their model output. SPX is supported by NOAA. IPRC/SOEST publication #xx/yy.

References

Adler RF, Huffman GJ, Chang A, Ferraro R, Xie P, Janowiak J, Rudolf B, Schneider U, Curtis S, Bolvin D, Gruber A, Susskind J, Arkin P (2003) The Version 2 Global Precipitation Climatology Project (GPCP) Monthly Precipitation Analysis (1979-Present). J. Hydrometeor 4:1147-1167

Bellucci A, Gualdi S, Navarra A (2010) The double-ITCZ syndrome in coupled general circulation models: The role of large-scale vertical circulation regimes. J Clim 23:1127–1145

Biasutti M, Sobel AH, Kushnir Y (2006) AGCM precipitation biases in the tropical At-lantic. J Clim 19:935–958

Breugem WP, Hazeleger W, Haarsma RJ (2006) Multimodel study of tropical Atlantic variability and change. Geophys Res Lett 33. doi:10.1029/2006GL027831

Caniaux G, Giordani H, Redelsperger J-L, Guichard F, Key E, Wade M (2011) Coupling between the Atlantic cold tongue and the West African monsoon in boreal spring and summer. J Geophys Res 116. doi:10.1029/2010JC00657

Carton JA, Huang B (1994) Warm events in the tropical Atlantic. J Phys Oceanogr 24:888–903

Carton JA, Chepurin G, Cao X, Giese BS (2000) A Simple Ocean Data Assimilation analysis of the global upper ocean 1950-95. Part I: Methodology. J Phys Oceanogr 30:311-326

Chang P, Ji L, Li H (1997) A decadal climate variation in the tropical Atlantic Ocean from thermodynamic air-sea interactions. Nature 385:516–518

Chang P, Coauthors (2006) Climate Fluctuations of Tropical Coupled Systems—The Role of Ocean Dynamics. J Clim 19:5122–5174

Chang CY, Carton JA, Grodsky SA, Nigam S (2007) Seasonal climate of the tropical Atlantic sector in the NCAR Community Climate System Model 3: error structure and probable causes of errors. J Clim 20:1053–1070

Chang CY, Nigam S, Carton JA (2008) Origin of the springtime westerly bias in equatorial Atlantic surface winds in the Community Atmosphere Model version 3 (CAM3) simulation. J Clim 21:4766-4778

Davey MK, Coauthors (2002) STOIC: a study of coupled model climatology and variability in topical ocean regions. Clim Dyn 18:403-420

Dee DP, Coauthors (2011) The ERA-Interim reanalysis: configuration and performance of the data assimilation system. Quart J R Meteorol Soc 137:553-597

de Szoeke SP, Xie S-P (2008) The tropical eastern Pacific seasonal cycle: Assessment of errors and mechanisms in IPCC AR4 coupled ocean–atmosphere general circulation models. J Clim 21:2573–2590

Ding H, Keenlyside NS, Latif M (2010) Equatorial Atlantic interannual variability: the role of heat content. J Geophys Res 115. doi:10.1029/2010JC006304

Doi T, Tozuka T, Sasaki H, Masumoto Y, Yamagata T (2007) Seasonal and interannual variations of oceanic conditions in the Angola Dome. J Phys Oceanogr 37, 2698-2713

Doi T, Vecchi G, Rosati A, Delworth T (2012) Biases in the Atlantic ITCZ in seasonal-interannual variations for a coarse- and a high-resolution coupled climate model. J Clim 25:5494–5511

Du Penhoat Y, Treguier A-M (1985) The seasonal linear response of the Atlantic Ocean. J Phys Oceanogr 15:316–329

Florenchie, P, Lutjeharms JRE, Reason CJC, Masson S, Rouault M (2003) The source of Bengula Niños in the South Atlantic Ocean. Geophys Res Lett 30. doi:10.1029/2003GL017,172

Folland CK, Palmer TN, Parker DE (1986) Sahel rainfall and world-wide sea temperatures. Nature 320:602-607

Franca C, Wainer I, De Mesquita AR, Goni GJ (2003) Planetary equatorial trapped waves in the Atlantic Ocean from TOPEX/POSEIDON altimetry, in Interhemispheric Water Exchange in the Atlantic Ocean, Elsevier Oceanogr. Ser., vol. 68, edited by G. J. Goni and P. Malanotte-Rizzoli, pp. 213– 232, Elsevier, New York.

Guiavarc'h C, Treguier AM, Vangriesheim A (2008) Remotely forced biweekly deep oscillations on the continental slope of the Gulf of Guinea. J Geophys Res 113. doi:10.1029/2007JC004471.

Hastenrath S, Heller L (1977) Dynamics of climate hazards in Northeast Brazil. Q J R Meteorol Soc 103:77-92

Hisard P, Henin C, Houghton R, Piton B, Rual P (1986) Oceanic conditions in the tropical Atlantic during 1983 and 1984. Nature 322:243–245

Hormann V, Brandt P (2009) Upper equatorial Atlantic variability during 2002 and 2005 associated with equatorial Kelvin waves. J Geophys Res 114(C03007). doi:10.1029/2008JC005101.

Illig S, Dewitte B, Ayoub N, du Penhoat Y, Reverdin G, De Mey P, Bonjean F, Lagerloef GSE (2004) Interannual long equatorial waves in the tropical Atlantic from a high-resolution ocean general circulation model experiment in 1981–2000. J Geophys Res 109(C02022). doi:10.1029/2003JC001771.

Jin F-F (1997) An equatorial ocean recharge paradigm for ENSO. Part I: Conceptual model. J Atmos Sci 54:811–829

Kalnay E, Coauthors (1996) The NCEP/NCAR 40-Year Reanalysis Project. Bull Amer Meteor Soc 77:437–471

Katz EJ (1997) Waves along the equator in the Atlantic. J Phys Oceanogr 27:2536 – 2544

Keenlyside NS, Latif M (2007) Understanding equatorial Atlantic interannual variability. J Clim 20:131-142

Li G, Xie S-P (2012) Origins of tropical-wide SST biases in CMIP multi-model ensembles. *Geophys Res Lett* 39, in press, doi:10.1029/2012GL053777

Lin JL (2007) The double-ITCZ problem in IPCC AR4 coupled GCMs: Ocean–atmosphere feedback analysis. J Clim 20:4497–4525

Locarnini RA, Mishonov AV, Antonov JI, Boyer TP, Garcia HE (2006) World Ocean Atlas 2005, Volume 1: Temperature. S. Levitus, Ed. NOAA Atlas NESDIS 61, U.S. Government Printing Office, Washington, D.C., 182 pp

Lubbecke JF, Boning CW, Keenlyside NS, Xie, S-P (2010) On the connection between Benguela and equatorial Atlantic Niños and the role of the South Atlantic anticyclone. J Geophys Res 115(C09015). doi:10.1029/2009JC005964.

Luo J-J, Masson S, Behera S, Yamagata T (2008) Extended ENSO predictions using a fully coupled ocean-atmosphere model. J Clim 21:84-93

Mechoso CR, Coauthors (1995) The seasonal cycle over tropical Pacific in coupled ocean–atmosphere general circulation models. Mon Weather Rev 123:2825–2838

Mitchell T, Wallace JM (1992) The annual cycle in equatorial convection and sea surface temperature. J Clim 5:1140–1156

Nobre P, Shukla J (1996) Variations of sea surface temperature, wind stress, and rainfall over the tropical Atlantic and South America. J Clim 9:2464-2479

Okumura Y, Xie S-P (2004) Interaction of the Atlantic equatorial cold tongue and African monsoon. J Clim 17:3588–3601

Okumura Y, Xie S-P (2006) Some overlooked features of tropical Atlantic climate leading to a new Nino-like phenomenon. J Clim 19:5859-5874

Philander SGH, Pacanowski RC (1981) The oceanic response to cross-equatorial winds (with application to coastal upwelling in low latitudes). Tellus 33:201-210

Philander SGH (1986) Unusual conditions in the tropical Atlantic Ocean in 1984. Nature 322:236–238

Philander SGH (1990) El Niño, La Niña, and the Southern Oscillation, Int Geophys Ser vol. 46, 293 pp., Academic, New York.

Polo I, Lazar A, Rodriguez-Fonseca B, Arnault S (2008) Oceanic Kelvin waves and tropical Atlantic intraseasonal variability: 1. Kelvin wave characterization. J Geophys Res 113(C07009). doi:10.1029/2007JC004495

Rayner NA, Parker DE, Horton EB, Folland CK, Alexander LV, Rowell DP, Kent EC, Kaplan A (2003) Global analyses of sea surface temperature, sea ice, and night marine air temperature since the late nineteenth century. J Geophys Res 108 (D14, 4407). doi10.1029/2002JD002670

Reynolds RW, Rayner NA, Smith TM, Stokes DC, Wang W (2002) An improved in situ and satellite SST analysis for climate. J Clim 15:1609-1625

Richter I, Xie S-P (2008) On the origin of equatorial Atlantic biases in coupled general circulation models. Clim Dyn 31:587-598

Richter I, Behera SK, Masumoto Y, Taguchi B, Komori N, Yamagata T (2010) On the triggering of Benguela Niños: Remote equatorial versus local influences. Geophys Res Lett 37(L20604). doi:10.1029/2010GL044461

Richter I, Xie S-P, Wittenberg AT, Masumoto Y (2012) Tropical Atlantic biases and their relation to surface wind stress and terrestrial precipitation. Clim Dyn 38:985-1001. doi: 10.1007/s00382-011-1038-9.

Richter I, Behera SK, Masumoto Y, Taguchi B, Sasaki H, Yamagata T (2012) Equatorial Atlantic warm events that do not rely on ENSO-like air-sea coupling. Nature Geosci, *accepted*

Ruiz-Barradas A, Carton JA, Nigam S (2000) Structure of interannual-to-decadal variability in the tropical Atlantic sector. J Clim 13:3285-3297

Servain J, Picaut J, Merle J (1982) Evidence of remote forcing in the equatorial Atlantic Ocean. J Phys Oceanogr 12:457–463

Servain J, Wainer I, McCreary JP, Dessier A (1999) Relationship between the Equatorial and meridional modes of climatic variability in the tropical Atlantic. Geophys Res Lett 26:485–488

Servain J, Wainer I, Ayina HL, Roquet H (2000) The relationship between the simulated climatic variability modes of the tropical Atlantic. Int J Climatol 20:939–953

Shannon LV, Boyd AJ, Bundrit GB, Taunton-Clark J (1986) On the existence of an El Niño–type phenomenon in the Benguela system. J Mar Sci 44:495–520

Stockdale TN, Balmaseda MA, Vidard A (2006) Tropical Atlantic SST prediction with coupled ocean-atmosphere GCMs. J Clim 19:6047-6061

Tokinaga H, Xie S-P (2011) Wave and Anemometer-based Sea-surface Wind (WASWind) for climate change analysis. J Clim 24:267-285

Tozuka, T, Doi T, Miyasaka T, Keenlyside N, Yamagata T (2011) Key factors in simulating the equatorial Atlantic zonal sea surface temperature gradient in a coupled general circulation model. J Geophys Res 116(C06010). doi:10.1029/2010JC006717, 2011

Uppala SM, Coauthors (2005) The ERA-40 re-analysis. Quart J R Meteorol Soc 131: 2961-3012. doi:10.1256/qj.04.176

Vauclair F, du Penhoat Y (2001) Interannual variability of the upper layer of the tropical Atlantic from in situ data between 1979 and 1999. Clim Dyn 17:527–546

Wahl S, Latif M, Park W, Keenlyside N (2009) On the Tropical Atlantic SST warm bias in the Kiel Climate Model. Clim Dyn, DOI 10.1007/s00382-009-0690-9

Woodruff SD, Coauthors (2011) ICOADS Release 2.5: Extensions and enhancements to the surface marine meteorological archive. Int J Climatol 31:951-967

Xie S-P, Philander SGH (1994) A coupled ocean-atmosphere model of relevance to the ITCZ in the eastern Pacific. Tellus 46A:340-350

Xie S-P, Carton JA (2004) Tropical Atlantic variability: Patterns, mechanisms, and impacts. In Earth Climate: The Ocean-Atmosphere Interaction, Wang C, Xie S-P, Carton JA (eds.), Geophysical Monograph, 147, AGU, Washington D.C., 121-142.

Zebiak SE (1993) Air–sea interaction in the equatorial Atlantic region. J Clim 6:1567–1586

Captions

A. Tables

Table 1. Coupled GCMs analyzed in this study. The second and third columns list the models selected for ensemble MOST and AN, respectively.

Table 2. AMIP GCMs analyzed in this study. Column two shows the names of corresponding coupled counterparts in piControl. Column three indicates which models are included in ensemble AMIP.

Table 3. AMIP GCMs analyzed in this study. Column two shows the names of corresponding coupled counterparts in piControl. Column three indicates which models are included in ensemble AMIP.

B. Figures

Fig. 1 Climatological annual mean SST along the equator averaged between 2°S-2°N for a CMIP5 pre-industrial Control simulations, and b CMIP3 pre-industrial Control simulations. The thick black line in both panels shows the OISST observations, the thick green line the ensemble average.

Fig. 2 Longitude-time sections of biases in SST (shading; K), surface wind stress (vectors; reference vector 0.2 Nm-2×E-1), and 20°C-isotherm depth (contours; interval 5 m) for the pre-industrial control simulations. All fields are meridionally averaged from 2°S to 2°N. Biases are in relative to OISST (SST), ICOADS based WAS-

Wind (surface wind stress), and World Ocean Atlas (20°C-isotherm depth). The panels show ensemble averages over a nearly all models, and b models with a relatively realistic representation of Atlantic Niños. See Table 1 for a definition of the model ensembles.

Fig. 3 Climatological MAM biases of precipitation (shading; mm d-1), and surface wind stress (vectors; reference vector 0.2 Nm-2×E-1) for a model ensemble of AMIP simulations. See Table 1 for a definition of the ensemble. Biases are with respect to GPCP precipitation and WASWind surface wind stress.

Fig. 4 Intermodel scatter plot of MAM precipitation averaged over the equatorial Amazon region (70-40°W, 0-5°N) and MAM equatorial surface zonal wind stress (averaged over 40-10°W, 2°S-2°N). Each letter corresponds to one dataset. “a” and “b” mark the observations and ERA40 reanalysis, respectively. Observations are GPCP precipitation and WASWind zonal wind stress. The black line shows a linear regression fit. Correlation coefficient and its square are displayed in the lower left.

Fig. 5 Intermodel scatter plots of climatological MAM precipitation south of the equator (40°W-10°E, 10-4°S) and MAM equatorial zonal surface wind stress (40-10°W, 2°S-2°N) for **a** AMIP simulations, and **b** pre-industrial control simulations. The regression line calculations exclude outliers (“e”, “j”, “s” for panel **a**, and flux-corrected models and “k”, “r”,”s” for panel **b**). Correlations are displayed in the lower right and upper left for panels **a** and **b**, respectively. Observations (letter “a”) are based on GPCP precipitation and WASWind zonal wind stress.

Fig. 6 Equatorial surface zonal wind stress (averaged over 40-10°E, 2°S-2°N) as a function of ITCZ latitude for **a** the ERA Interim reanalysis (left panel), and **b** the pre-industrial control MOST ensemble. ITCZ latitude was calculated based on monthly mean precipitation and used to composite the concomitant zonal wind stress index. See text for details. The blue shading in panel b indicates the 95% confidence level based on the inter-ensemble variance.

Fig. 7 First EOF of seasonally averaged JJA SST (shading; K) in the HadISST, ERA40, ensemble AN, MOST-AN, which excludes AN models, and individual AN members (bottom two rows). The PC was normalized such that the EOF indicates amplitude. The respective explained variance is indicated at the top of each panel, except for ensemble means. The upper two rows additionally show surface wind (vectors; reference 0.5 m s-1 per standard deviation) and precipitation (contours; interval 0.3 mm d-1 per standard deviation) regressed on the principal component of the first SST EOF.

Fig. 8 Longitude-time sections of interannual standard deviation of SST (shading; K), and surface zonal wind stress (contours; interval 0.2 Nm-2×E-2). Both fields are averaged from 2°S to 2°N. The individual panels show **a** ERA Interim reanalysis, **b** ERA 40 reanalysis, **c** ensemble MOST-AN, and **d** ensemble AN.

Fig. 9 Correlation calculated for observations, reanalysis, pre-industrial control simulations for the following anomaly fields. **a** MAM equatorial surface zonal wind stress (averaged over 40-10°E, 2°S-2°N) and JJA cold tongue SST (15-5°W, 3°S-3°N), and **b** JJA cold tongue SST and MAM meridional SST gradient (30°W-10°E, 18-6°S minus 80-10°W, 6-18°N. Models belonging to ensemble AN are marked with a blue rectangle.

Fig. 10 Composite evolution of anomalous surface zonal wind stress (40-10°E, 2°S-2°N; green line), SST (15-5°W, 3°S-3°N; blue line), 20°C-isotherm depth (15-5°W, 3°S-3°N; orange line), and precipitation (40°W-10°E, 10-4°S; red line). The criterion for compositing was based on 1.5 standard deviations of JJA SST in the cold tongue region (15-5°W, 3°S-3°N). All fields have been normalized by their respective standard deviations. The panels show **a** ICOADS, **b** ERA40, **c** ERA Interim, **d** SODA, **e** the ensemble average over models with one-stage Atlantic Niños, and **f** the ensemble average over models with two-stage Atlantic Niños (see text for details).

Fig. 11 Anomalies of precipitation (shading; mm d-1), surface winds (vectors; reference 2 m s-1), and SST (contours; interval 0.2 K), composited on MAM surface zonal wind anomalies along the equator (40-10°W, 2°S-2°N) that exceed 2.5 standard deviations. The panels show **a** ERA40 reanalysis, and **b** ensemble AN.

Fig. 12 Latitude-time sections of climatological precipitation (shading; mm d-1) and surface wind stress (vectors; reference 5 Nm-2×E-2) averaged between (40-30°W). The panels show **a** GPCP precipitation and WASWind surface wind stress, **b** ERA Interim reanalysis, **c** ensemble MOST, **d** ensemble AN. The orange contour lines in panels b, c, and d show the precipitation difference with the GPCP climatology.

A. Tables

model	ensemble MOST	ensemble AN
ACCESS1-0	x	
ACCESS1-3	x	x
bcc-csm1-1	x	x
BNU-ESM	x	
CanESM2	x	
CCSM4	x	
CNRM-CM5		
CSIRO-Mk3-6-0	x	
EC-EARTH	x	
FGOALS-g2	x	
FGOALS-s2	x	
FIO-ESM	x	
GFDL-CM3	x	x
GFDL-ESM2G	x	
GFDL-ESM2M	x	x
GISS-E2-H	x	
GISS-E2-R	x	
HadGEM2-CC		
HadGEM2-ES	x	x
inmcm4	x	
IPSL-CM5A-LR		
IPSL-CM5A-MR		
IPSL-CM5B-LR		
MIROC4h	x	
MIROC5	x	x
MIROC-ESM	x	
MIROC-ESM-CHEM		
MPI-ESM-LR	x	
MPI-ESM-MR	x	
MPI-ESM-P		
MRI-CGCM3	x	x
NorESM1-M	x	x
NorESM1-ME		

Table 1. Coupled GCMs analyzed in this study. The second and third columns list the models selected for ensemble MOST and AN, respectively.

model	piControl counterpart	ensemble AMIP
bcc-csm1-1	bcc-csm1-1	x
CanAM4	CanESM2	x
CNRM-CM5	CNRM-CM5	
CSIRO-Mk3-6-0	CSIRO-Mk3-6-0	
EC-EARTH	EC-EARTH	
FGOALS-s2	FGOALS-s2	x
GFDL-ESM2M	gfdl_cm2_1 (CMIP3)	x
GFDL-HIRAM-C180		
GFDL-HIRAM-C360		
GISS-E2-R	GISS-E2-R	x
HadGEM2-ES	HadGEM2-A	x
inmcm4	inmcm4	x
IPSL-CM5A-LR	IPSL-CM5A-LR	
MIROC5	MIROC5	x
MPI-ESM-LR	MPI-ESM-LR	x
MPI-ESM-MR	MPI-ESM-MR	x
MRI-AGCM3-2H		
MRI-AGCM3-2S		
MRI-CGCM3	MRI-CGCM3	x
NorESM1-M	NorESM1-M	x

Table 2. AMIP GCMs analyzed in this study. Column two shows the names of corresponding coupled counterparts in piControl. Column three indicates which models are included in ensemble AMIP.

model	1-stage Niño	2-stage Niño	ensemble AN
ACCESS1-0		x	
ACCESS1-3	x		x
bcc-csm1-1		x	x
BNU-ESM		x	
CanESM2	x		
CCSM4		x	
CSIRO-Mk3-6-0	x		
FGOALS-g2			
FGOALS-s2			
FIO-ESM			
GFDL-CM3		x	x
GFDL-ESM2G			
GFDL-ESM2M		x	x
GISS-E2-R	x		
HadGEM2-ES		x	x
inmcm4	x		
MIROC4h	x		
MIROC5		x	x
MIROC-ESM	x		
MPI-ESM-LR		x	
MRI-CGCM3		x	x
NorESM1-M		x	x

Table 3. AMIP GCMs analyzed in this study. Column two shows the names of corresponding coupled counterparts in piControl. Column three indicates which models are included in ensemble AMIP.

Figure 1

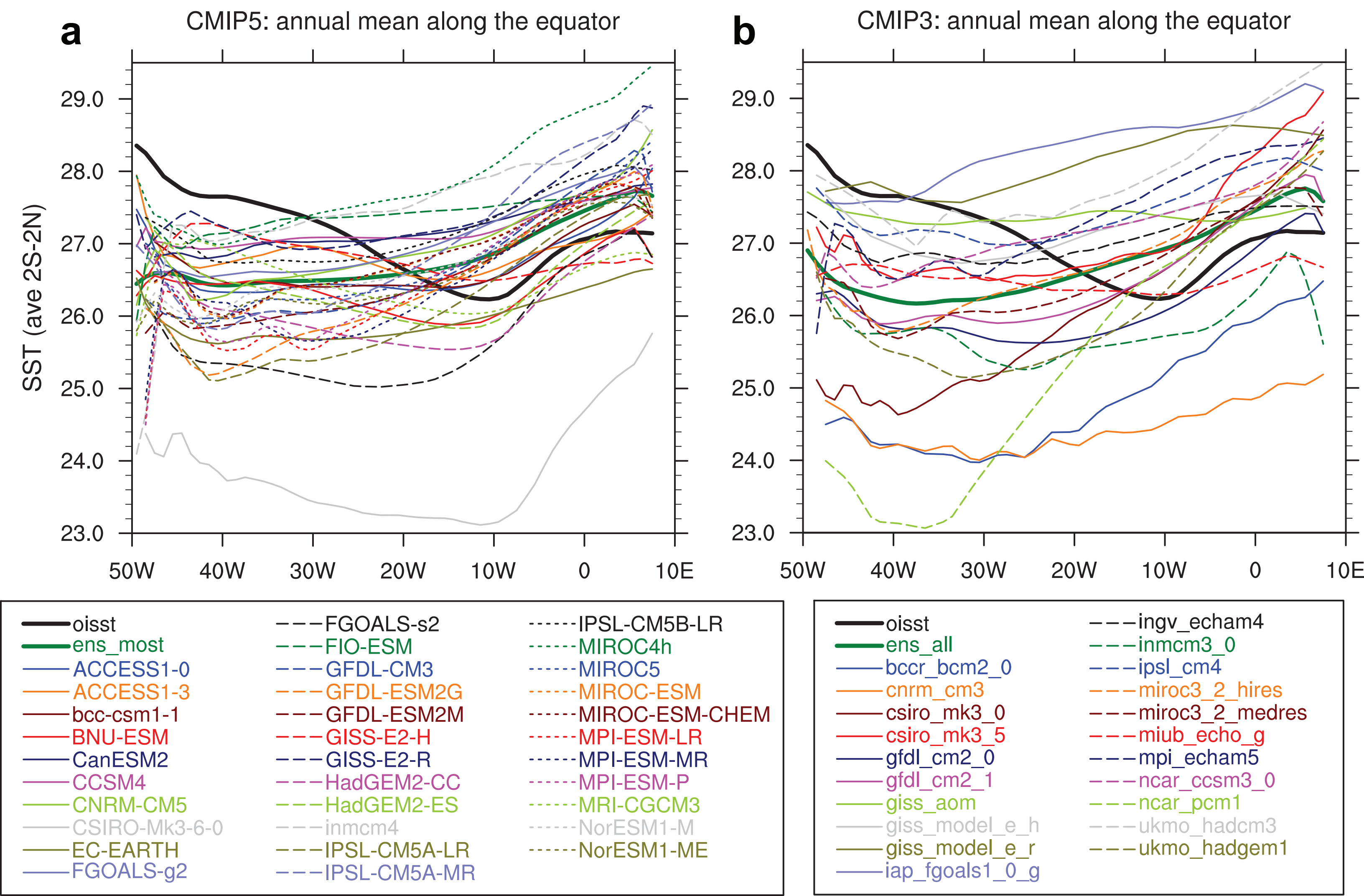

a
CMIP5: annual mean along the equator
b
CMIP3: annual mean along the equator
SST (ave 2S-2N)
29.0
28.0
27.0
26.0
25.0
24.0
23.0
50W
40W
30W
20W
10W
0
10E
oisst
ens_most
ACCESS1-0
ACCESS1-3
bcc-csm1-1
BNU-ESM
CanESM2
CCSM4
CNRM-CM5
CSIRO-Mk3-6-0
EC-EARTH
FGOALS-g2
FGOALS-s2
FIO-ESM
GFDL-CM3
GFDL-ESM2G
GFDL-ESM2M
GISS-E2-H
GISS-E2-R
HadGEM2-CC
HadGEM2-ES
inmcm4
IPSL-CM5A-LR
IPSL-CM5A-MR
IPSL-CM5B-LR
MIROC4h
MIROC5
MIROC-ESM
MIROC-ESM-CHEM
MPI-ESM-LR
MPI-ESM-MR
MPI-ESM-P
MRI-CGCM3
NorESM1-M
NorESM1-ME
oisst
ens_all
bccr_bcm2_0
cnrm_cm3
csiro_mk3_0
csiro_mk3_5
gfdl_cm2_0
gfdl_cm2_1
giss_aom
giss_model_e_h
giss_model_e_r
iap_fgoals1_0_g
ingv_echam4
inmcm3_0
ipsl_cm4
miroc3_2_hires
miroc3_2_medres
miub_echo_g
mpi_echam5
ncar_ccsm3_0
ncar_pcm1
ukmo_hadcm3
ukmo_hadgem1

Figure 2

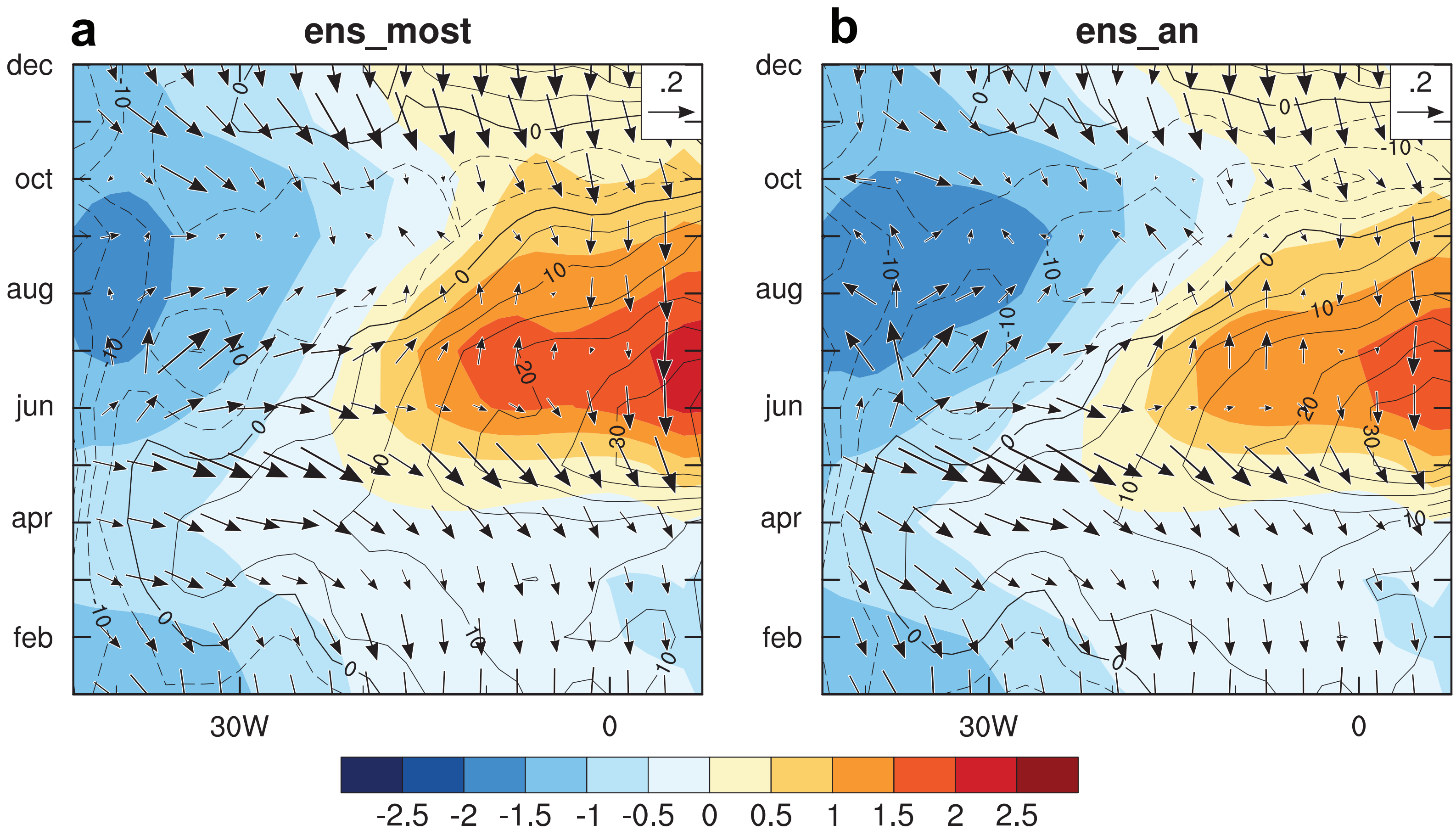
a
ens_most
b
ens_an
dec
oct
aug
jun
apr
feb
30W
0
.2
-2.5 -2 -1.5 -1 -0.5 0 0.5 1 1.5 2 2.5

Figure 3

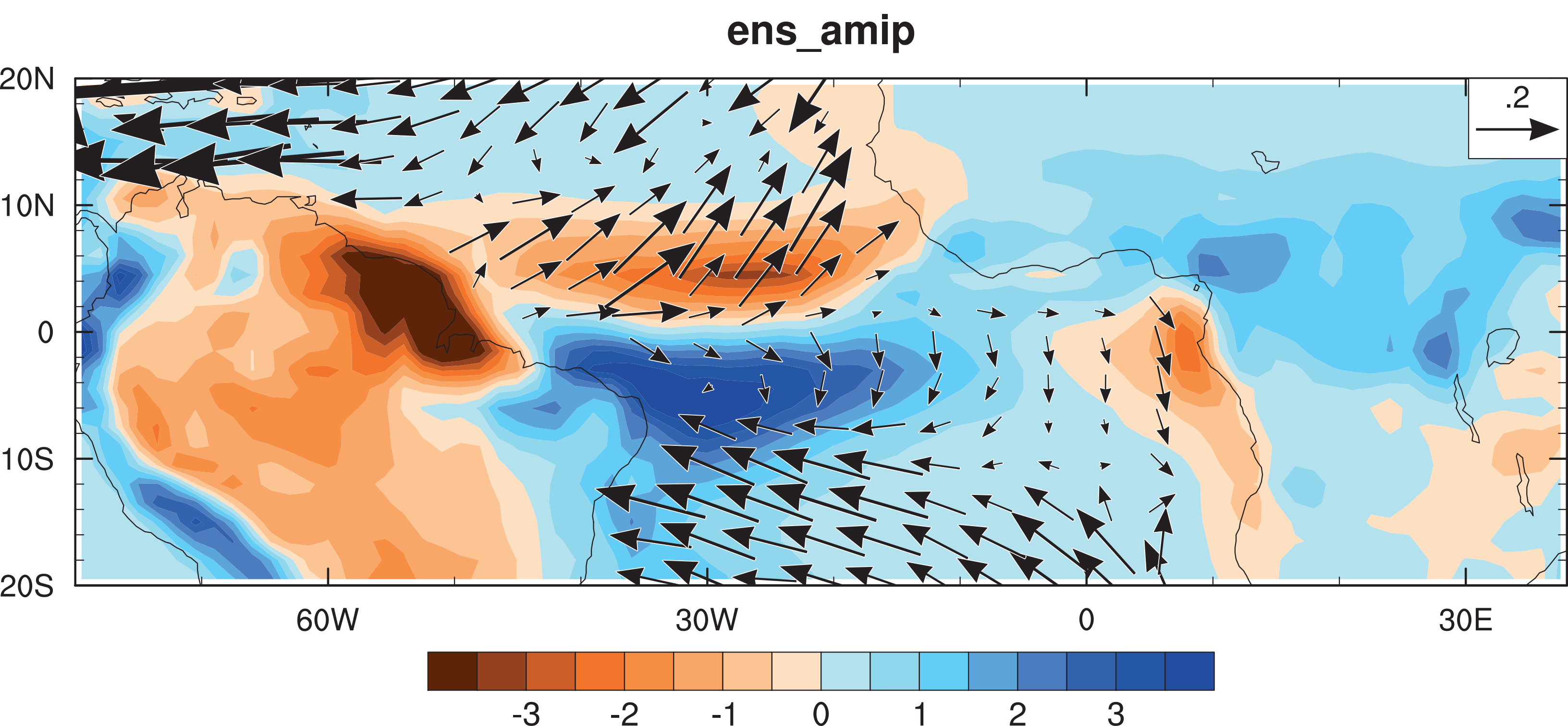

Figure 4

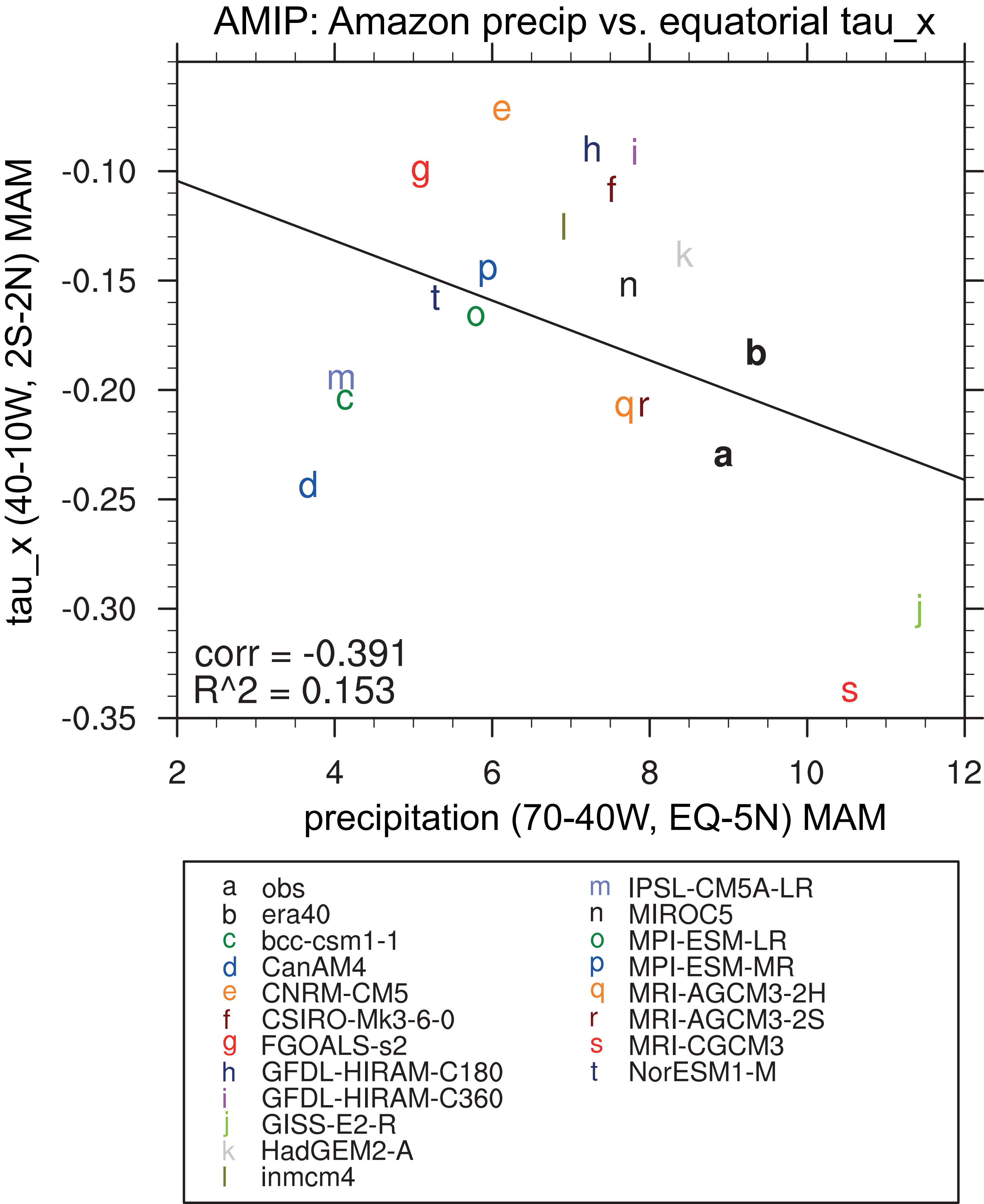
AMIP: Amazon precip vs. equatorial tau_x
tau_x (40-10W, 2S-2N) MAM
precipitation (70-40W, EQ-5N) MAM
-0.10
-0.15
-0.20
-0.25
-0.30
-0.35
2
4
6
8
10
12
corr = -0.391
R^2 = 0.153
a obs
b era40
c bcc-csm1-1
d CanAM4
e CNRM-CM5
f CSIRO-Mk3-6-0
g FGOALS-s2
h GFDL-HIRAM-C180
i GFDL-HIRAM-C360
j GISS-E2-R
k HadGEM2-A
l inmcm4
m IPSL-CM5A-LR
n MIROC5
o MPI-ESM-LR
p MPI-ESM-MR
q MRI-AGCM3-2H
r MRI-AGCM3-2S
s MRI-CGCM3
t NorESM1-M

Figure 5

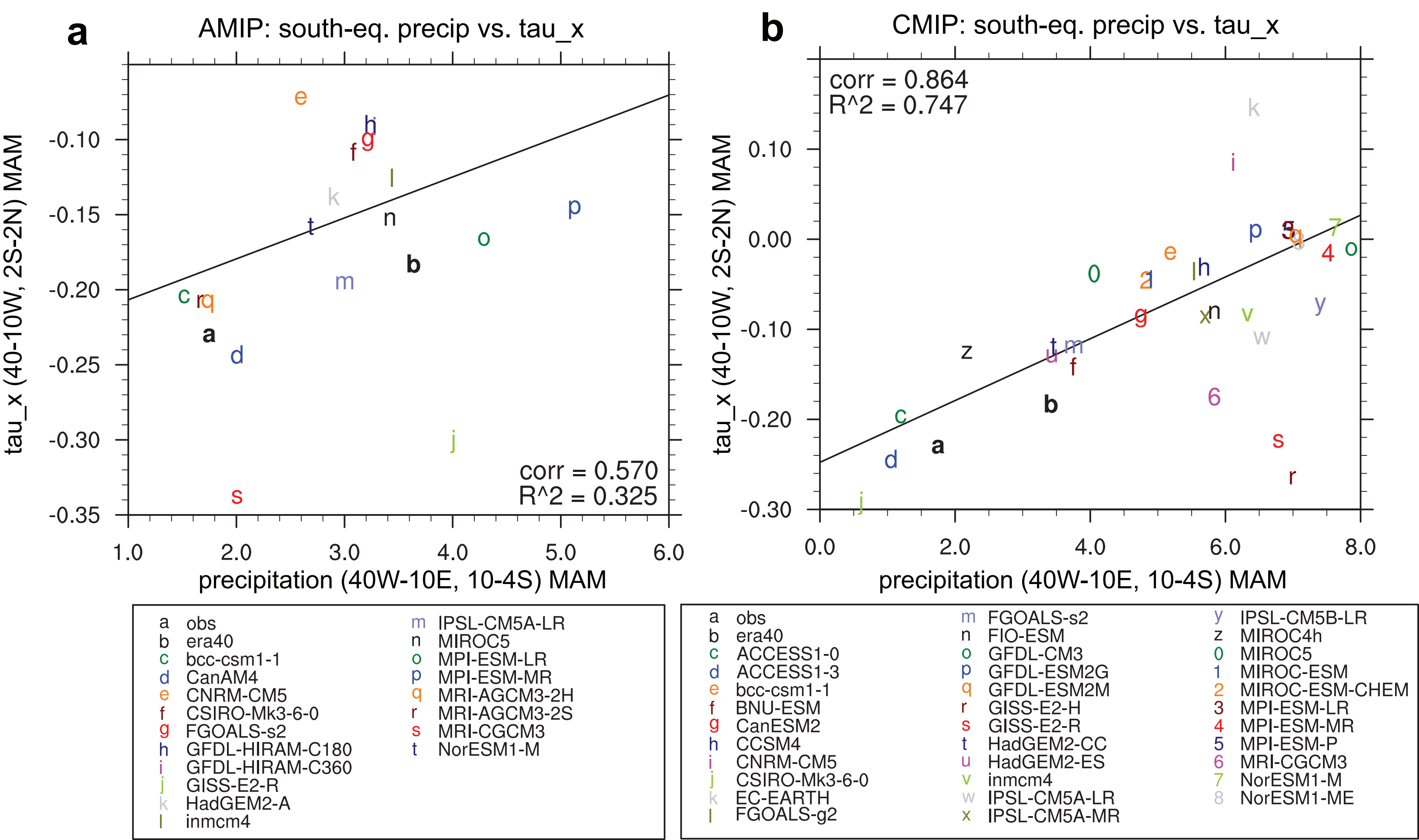
a
AMIP: south-eq. precip vs. tau_x
corr = 0.570
R^2 = 0.325
tau_x (40-10W, 2S-2N) MAM
precipitation (40W-10E, 10-4S) MAM
b
CMIP: south-eq. precip vs. tau_x
corr = 0.864
R^2 = 0.747
tau_x (40-10W, 2S-2N) MAM
precipitation (40W-10E, 10-4S) MAM
a obs
b era40
c bcc-csm1-1
d CanAM4
e CNRM-CM5
f CSIRO-Mk3-6-0
g FGOALS-s2
h GFDL-HIRAM-C180
i GFDL-HIRAM-C360
j GISS-E2-R
k HadGEM2-A
l inmcm4
m IPSL-CM5A-LR
n MIROC5
o MPI-ESM-LR
p MPI-ESM-MR
q MRI-AGCM3-2H
r MRI-AGCM3-2S
s MRI-CGCM3
t NorESM1-M
a obs
b era40
c ACCESS1-0
d ACCESS1-3
e bcc-csm1-1
f BNU-ESM
g CanESM2
h CCSM4
i CNRM-CM5
j CSIRO-Mk3-6-0
k EC-EARTH
l FGOALS-g2
m FGOALS-s2
n FIO-ESM
o GFDL-CM3
p GFDL-ESM2G
q GFDL-ESM2M
r GISS-E2-H
s GISS-E2-R
t HadGEM2-CC
u HadGEM2-ES
v inmcm4
w IPSL-CM5A-LR
x IPSL-CM5A-MR
y IPSL-CM5B-LR
z MIROC4h
0 MIROC5
1 MIROC-ESM
2 MIROC-ESM-CHEM
3 MPI-ESM-LR
4 MPI-ESM-MR
5 MPI-ESM-P
6 MRI-CGCM3
7 NorESM1-M
8 NorESM1-ME

Figure 6

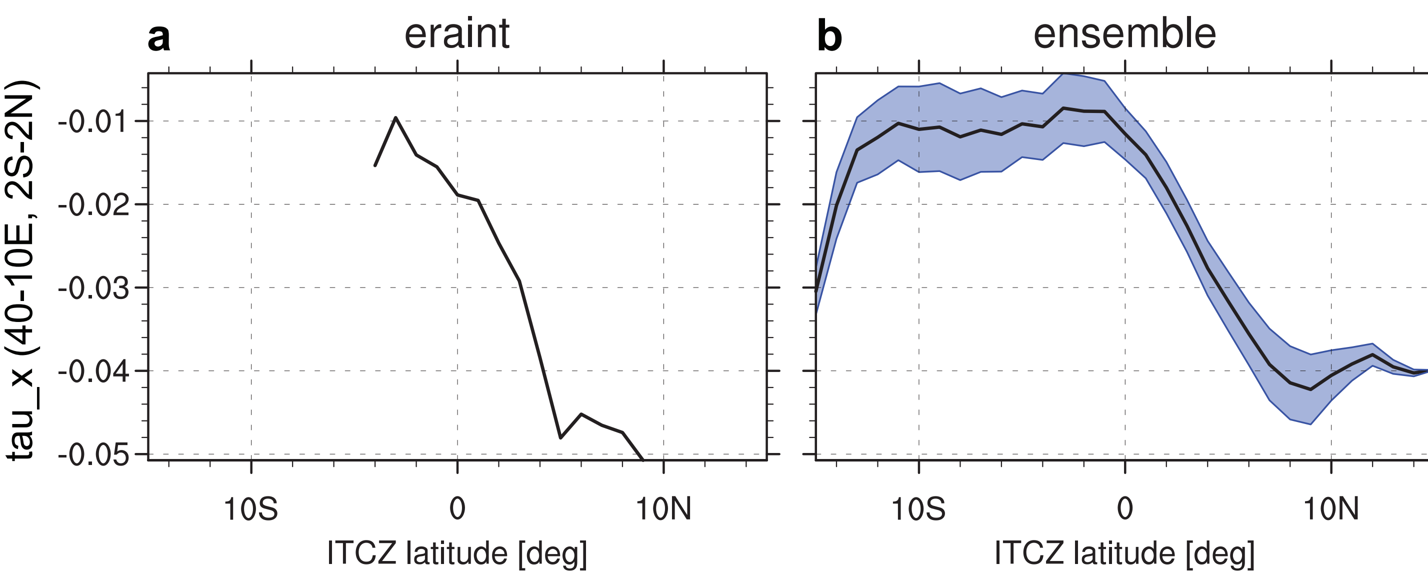

a
eraint
b
ensemble
tau_x (40-10E, 2S-2N)
-0.01
-0.02
-0.03
-0.04
-0.05
10S
0
10N
ITCZ latitude [deg]
10S
0
10N
ITCZ latitude [deg]

Figure 7

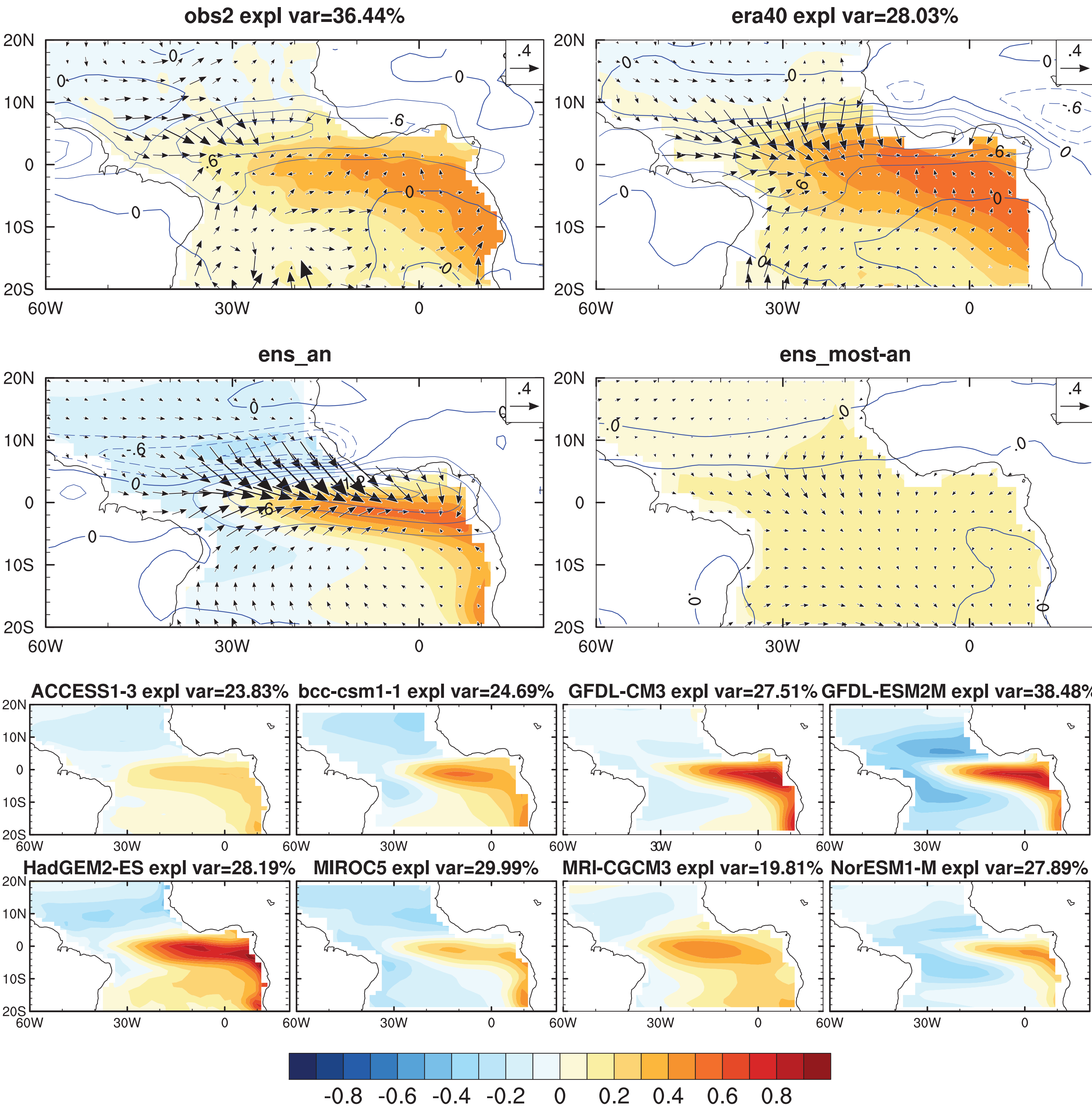

obs2 expl var=36.44%
era40 expl var=28.03%
ens_an
ens_most-an
ACCESS1-3 expl var=23.83%
bcc-csm1-1 expl var=24.69%
GFDL-CM3 expl var=27.51%
GFDL-ESM2M expl var=38.48%
HadGEM2-ES expl var=28.19%
MIROC5 expl var=29.99%
MRI-CGCM3 expl var=19.81%
NorESM1-M expl var=27.89%
20N
10N
0
10S
20S
60W
30W
0
.4
-0.8 -0.6 -0.4 -0.2 0 0.2 0.4 0.6 0.8

Figure 8

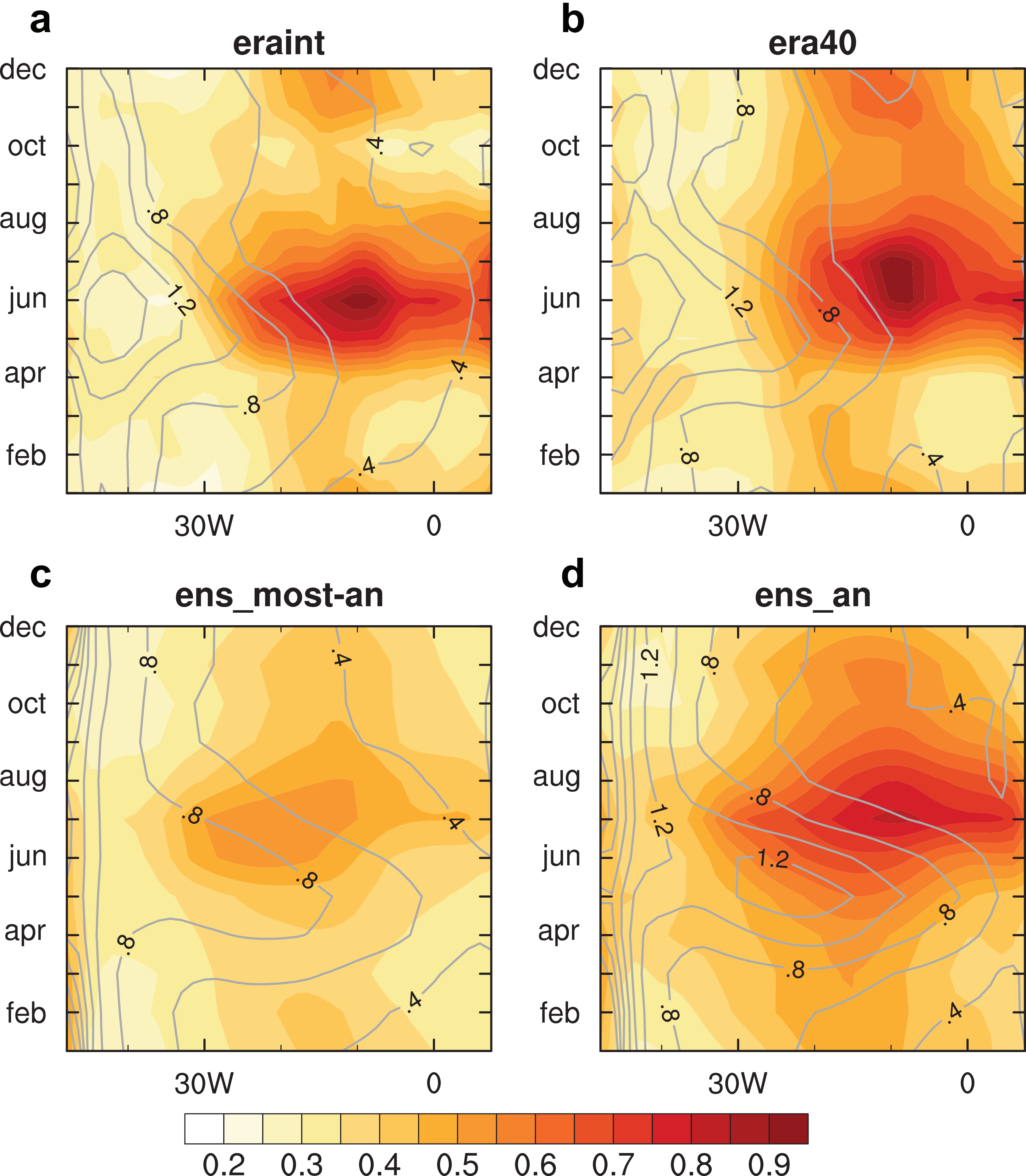
a
eraint
b
era40
c
ens_most-an
d
ens_an
dec
oct
aug
jun
apr
feb
30W
0
.8
1.2
.4
0.2
0.3
0.4
0.5
0.6
0.7
0.8
0.9

Figure 9

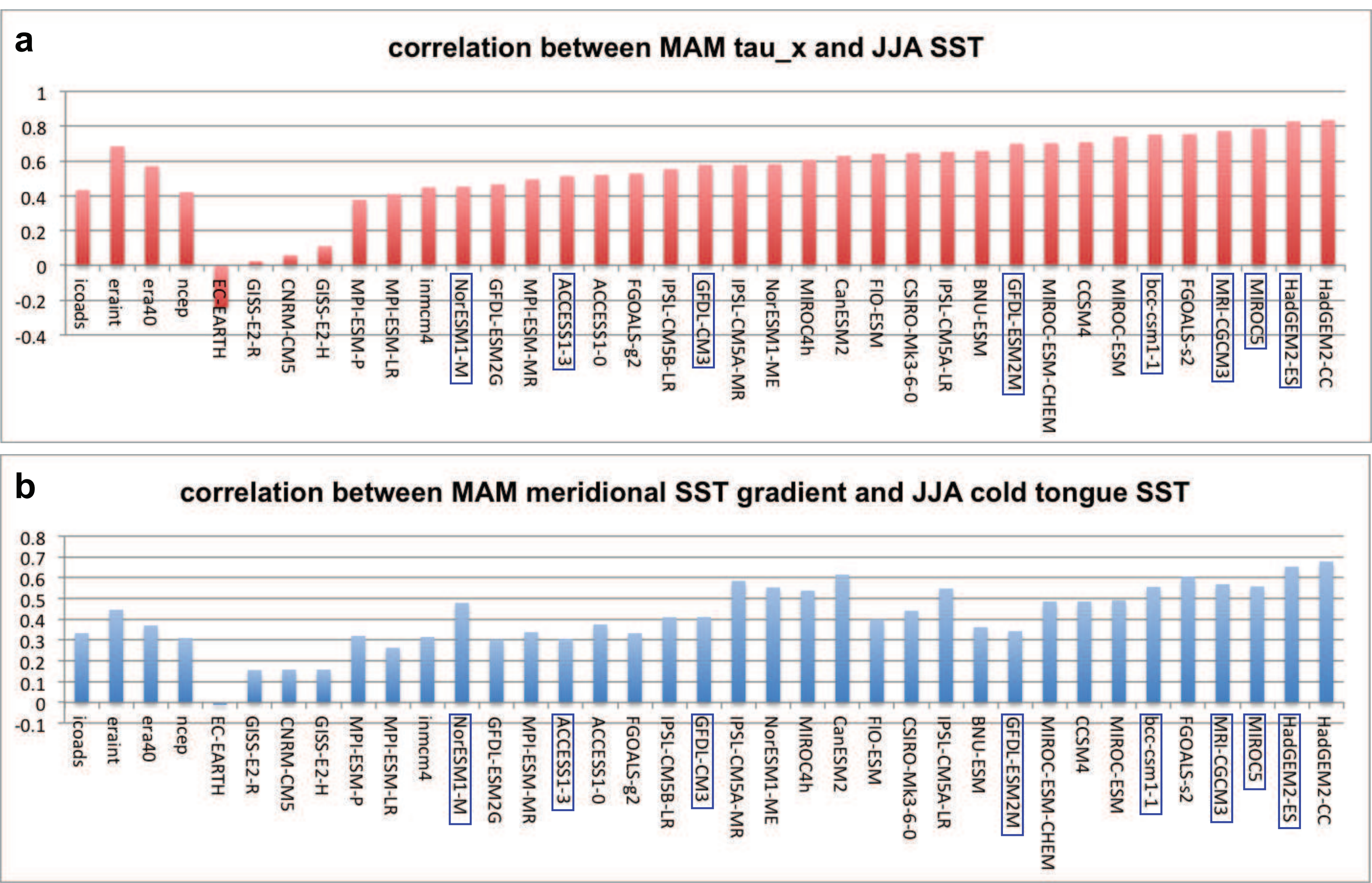
a
correlation between MAM tau_x and JJA SST
1
0.8
0.6
0.4
0.2
0
-0.2
-0.4
icoads
eraint
era40
ncep
EC-EARTH
GISS-E2-R
CNRM-CM5
GISS-E2-H
MPI-ESM-P
MPI-ESM-LR
inmcm4
NorESM1-M
GFDL-ESM2G
MPI-ESM-MR
ACCESS1-3
ACCESS1-0
FGOALS-g2
IPSL-CM5B-LR
GFDL-CM3
IPSL-CM5A-MR
NorESM1-ME
MIROC4h
CanESM2
FIO-ESM
CSIRO-Mk3-6-0
IPSL-CM5A-LR
BNU-ESM
GFDL-ESM2M
MIROC-ESM-CHEM
CCSM4
MIROC-ESM
bcc-csm1-1
FGOALS-s2
MRI-CGCM3
MIROC5
HadGEM2-ES
HadGEM2-CC
b
correlation between MAM meridional SST gradient and JJA cold tongue SST
0.8
0.7
0.6
0.5
0.4
0.3
0.2
0.1
0
-0.1
icoads
eraint
era40
ncep
EC-EARTH
GISS-E2-R
CNRM-CM5
GISS-E2-H
MPI-ESM-P
MPI-ESM-LR
inmcm4
NorESM1-M
GFDL-ESM2G
MPI-ESM-MR
ACCESS1-3
ACCESS1-0
FGOALS-g2
IPSL-CM5B-LR
GFDL-CM3
IPSL-CM5A-MR
NorESM1-ME
MIROC4h
CanESM2
FIO-ESM
CSIRO-Mk3-6-0
IPSL-CM5A-LR
BNU-ESM
GFDL-ESM2M
MIROC-ESM-CHEM
CCSM4
MIROC-ESM
bcc-csm1-1
FGOALS-s2
MRI-CGCM3
MIROC5
HadGEM2-ES
HadGEM2-CC

Figure 10

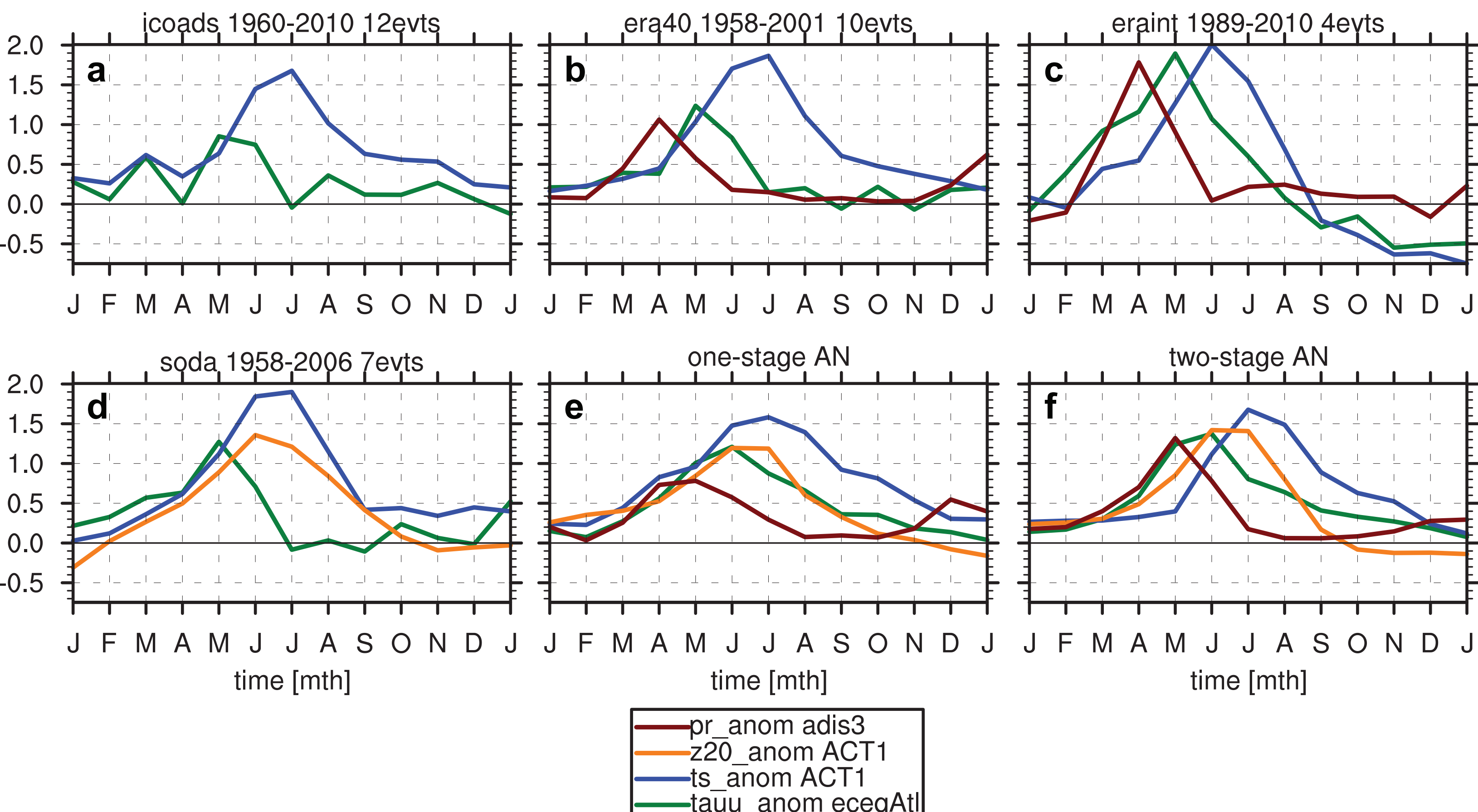

icoads 1960-2010 12evts
era40 1958-2001 10evts
eraint 1989-2010 4evts
soda 1958-2006 7evts
one-stage AN
two-stage AN
a
b
c
d
e
f
2.0
1.5
1.0
0.5
0.0
-0.5
J F M A M J J A S O N D J
time [mth]
pr_anom adis3
z20_anom ACT1
ts_anom ACT1
tauu_anom eceqAtl

Figure 11

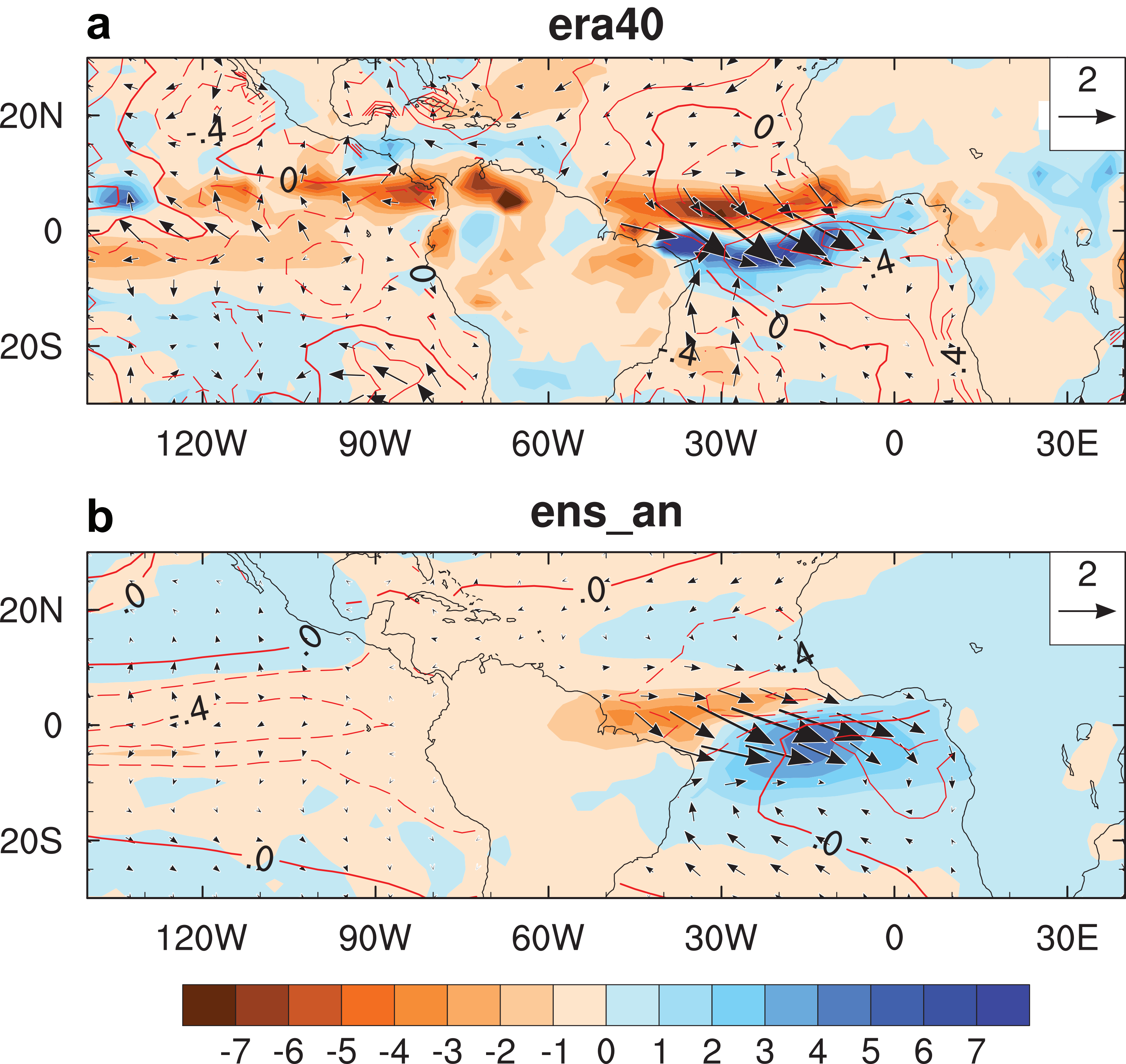
a
era40
2
20N
0
20S
120W
90W
60W
30W
0
30E
b
ens_an
2
20N
0
20S
120W
90W
60W
30W
0
30E
-7 -6 -5 -4 -3 -2 -1 0 1 2 3 4 5 6 7

Figure 12

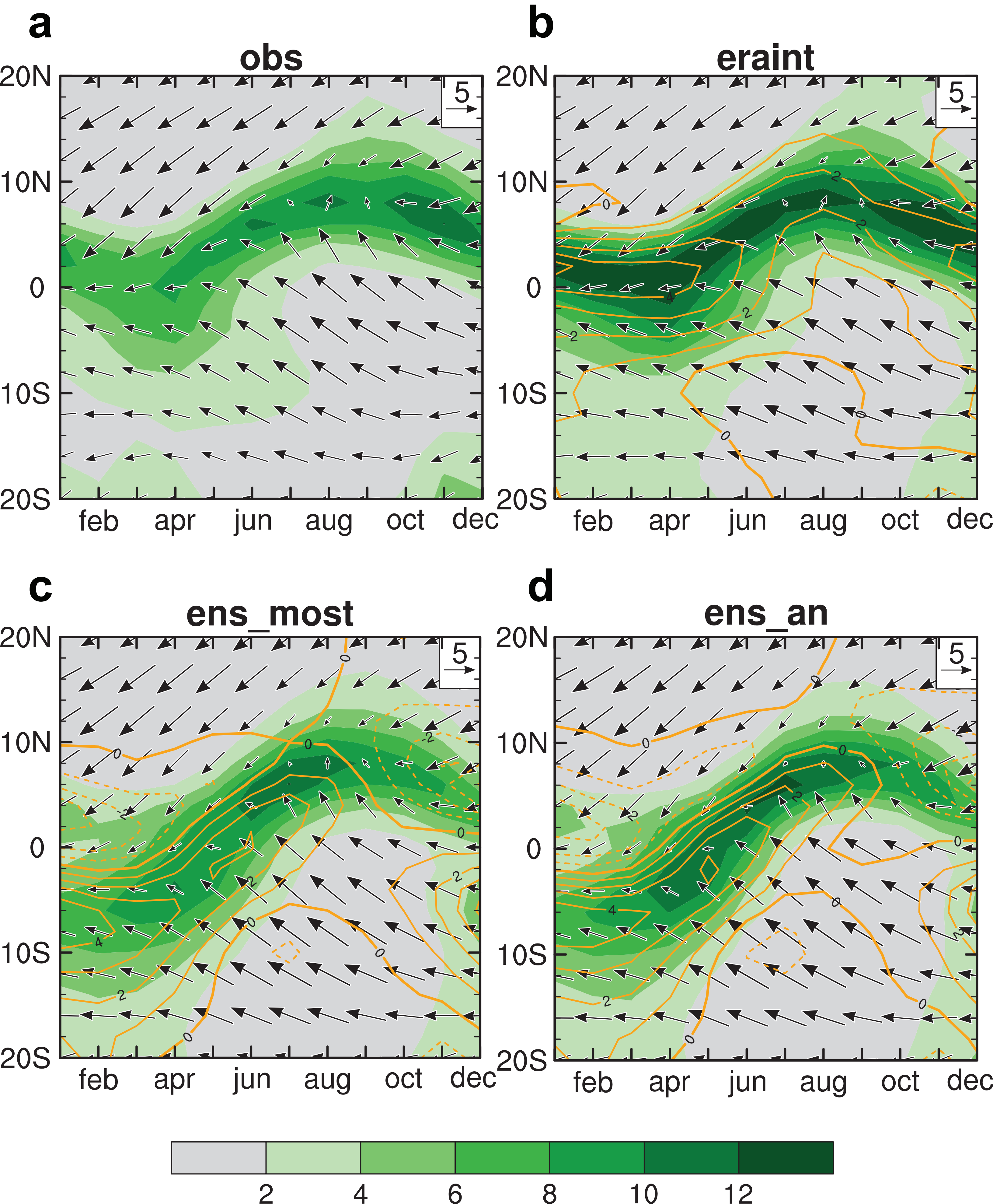

a
obs
b
eraint
c
ens_most
d
ens_an
20N
10N
0
10S
20S
feb
apr
jun
aug
oct
dec
5
2
4
6
8
10
12